INTERNATIONAL JOURNAL OF AUTOMOTIVE SCIENCE AND TECHNOLOGY

2024, VOL. 8, NO:4, 506-526

www.ijastech.org

e-ISSN: 2587-0963

$PI^{\lambda}D^{\mu}$ Controllers for Suppression of Limit Cycle in a Plant with Time Delay and Backlash Nonlinearity

Biresh Kumar Dakua [1*] and Bibhuti Bhusan Pati [1]

[1.] *Department of Electrical Engineering, Veer Surendra Sai University of Technology, Burla, Odisha, India*

Research Article

Abstract

This paper evaluates the existence of a periodic limit cycle oscillation in a system with backlash nonlinearity in the presence of time delay. An armature voltage-controlled DC motor system is studied in this regard whose output signifies accuracy in position control. An analytical solution for the limit cycle based on the Describing Function (DF) method is obtained whose authenticity is verified with the Nyquist contour-based graphical method and the digital simulations. The effect of parametric changes on the magnitude and frequency of the limit cycle is examined in this article. Integer and non-integer order proportional-integral-derivative (PID) controllers are designed to eliminate these undesirable periodic oscillations present in the system. Multiple optimization techniques considering error-based, time domain specification-based objective functions are scrutinized through statistical tests towards the parameter estimation of the applied controllers. Observations reveal that while the Moth flame optimizer (MFO) with Integral time absolute error (ITAE) produces superior results for the PID controller, the MFO with the Integral time square error (ITSE) provides better results for the FOPID controller. Further, the gain and phase margin-based loop shaping method is also used for an analytical calculation of the controller parameters. Out of the five loop shaping constraints, superior results are obtained by considering robustness towards gain variation constraint as an objective function, and the rest as nonlinear constraints. Simulation studies suggest the efficiency of the utilized controllers in quenching the periodic limit cycle oscillations. The superiority of the FOPID controller over the PID controller is validated by considering suitable performance-based comparisons. The effectiveness of the designed controllers is also tested against the variations in system parameters. Further, the physical realizations of the integer and fractional order PID controllers are performed through Oustaloup recursive filter approximation.

Keywords: Describing function; FOPID controllers; Limit cycle; Nonlinear Systems; Time-delay systems

History
Received 22.04.2024
Revised 01.09.2024
Accepted 11.09.2024

Contact
* Corresponding author
Biresh Kumar Dakua
bireshdakua@gmail.com
Address: Department of Electrical Engineering, Veer Surendra Sai University of Technology, Burla, Odisha, India
Tel: +91-9938948245

To cite this paper: Dakua, B.K., Pati, B.B.,. $PI^{\lambda}D^{\mu}$ Controllers for Suppression of Limit Cycle in a Plant with Time Delay and Backlash Nonlinearity. International Journal of Automotive Science and Technology. 2024; 8 (4): 506-526. https://doi.org/10.30939/ijastech..1471847

1. Introduction

Periodic sustained oscillations having constant magnitude and frequency exhibited by Nonlinear systems are called limit cycles. Although a nonlinear system shows a variety of phenomena like jump resonance, chaos, subharmonic oscillations, etc., the stability of the control system consisting of nonlinearities is commonly measured by the evaluation of limit cycle oscillation. Physical dynamical systems comprising various memory or non-memory type nonlinearities such as relay, saturation, dead zone, backlash, hysteresis etc., usually oscillate with a fixed amplitude and frequency regardless of any specific initial condition or zero initial condition. These limit cycles can sometimes be stable, semi-stable, or unstable. Being a periodic oscillation, limit cycles create problems in system control and obtaining desired system performance. Therefore, the problem of prediction and elimination of limit cycle is vital in the studies of nonlinear dynamical systems. The DF based approach is an efficient method used for the evaluation of nonlinear dynamical systems and thereby the analysis of periodic oscillations.

The input-output relationship-based DF method along with the Nyquist contour is used for the evaluation of the limit cycle in a linear time-delay system with backlash nonlinearity [1,2]. The DF-based procedure along with the Nyquist plot is been followed for the evaluation of the periodic oscillations in the case of Single Input Single Output (SISO) integer-order systems with backlash nonlinearity [3]. Similar observations regarding limit cycles using the Nyquist plots are also reported in [4,5]. An input-dependent Nyquist plot for the investigation of periodic oscillations in a system with multiple nonlinearities is described in [6]. The use of dual input describing function (DIDF) for the prediction of the limit cycle is presented in [7]. Extension of the above concepts toward the presence of a limit cycle in the non-integer (fractional) order systems is also reported in the literature. Periodic oscillations in fractional order systems with relay nonlinearity are provided in [8] by using the DF method along with digital simulations. Similarly, the evaluation of the limit cycle through Tsypkin's locus and DF method is mentioned in [9]. A novel A-locus method accompanying DF for the analysis of periodic oscillations is reported in [10,11]. The evaluation of the limit cycle in a fractional system with different static as well as dynamic nonlinearities is presented in [12]. An extension of this DF concept along with a graphical phasor diagram method towards the Two Input Two Output (TITO) system is provided in [13,14]. Although reasonable work has been done in the field of prediction of limit cycle in the case of both integer and fractional order systems as well as for various nonlinear elements; a very scant literature talks about periodic oscillations in MIMO nonlinear systems [15,16].

Elimination of these periodic limit cycle oscillations in nonlinear systems is a major challenge. Very few methods like the application of dither signal by considering Dual Input Describing Function (DIDF) for limit cycle suppression are discussed in the literature [7,13]. The PID controller is simpler and provides an efficient solution to real-world control problems. It effectively addresses both transients as well as the steady-state performances of the system. Due to the design simplicity, robustness, and near-optimal performance of PID, these are widely used in academic and industrial sectors [19-23]. Again, for the advancement in computational techniques, research on fractional calculus is in progress [24,25] and fractional PID (FOPID) controllers are found to outplay their integer counterparts [26]. To have a physical realization of the fractional elements various methods like the Oustaloup filter [27], and continued fractional expansion (CFE) are also reported [28,29]. The use of integer and non-integer order controllers for the elimination of periodic oscillations is demonstrated in [3,4,5, and 6]. State feedback-based pole placement techniques for the quenching of the limit cycle are shown in [14]. The research gap and motivation behind this study is the lack of proposed strategies for the quenching of the limit cycle oscillations.

Parameter estimation methods for the PID and FOPID controllers are demonstrated in many pieces of literature. Ziegler-Nichol's method, Pole placement method, Loop shaping method, and optimization techniques are some of the commonly used methods for the estimation of optimal parameters of these controllers [30,31]. The parameter estimation of non-integral order controllers is demonstrated by the minimization of square error in [32], sine-based auto-tuning methods [33], and the gain and phase margin-based loop shaping method [34-37], and the time-domain-based objective functions minimization in [38-41] respectively. The application of integer and non-integer order controllers for eliminating limit cycle, as well as frequency domain-based tuning strategy for obtaining desired performance in terms of relative stability, bandwidth, steady-state accuracy, robustness to parameter variations, and suppression of noise and disturbances, is the novelty of this research article.

The prime objective of this article is to predict and eliminate the periodic oscillations in the presence of backlash nonlinearity by applying PID and FOPID controllers. In this current work, the prediction of the limit cycle is carried out by an analytical method which was verified by graphical phasor diagrams as well as digital simulations. Integer and non-integer-order PID controllers are designed considering several optimization techniques like Whale Optimization Algorithm (WOA) [42], Particle Swarm Optimization (PSO) [43], Ant Lion Optimization (ALO) [44], Grey Wolf Optimization (GWO) [45], and Moth Flame Optimization (MFO) [46] and multiple objective functions such as Integral Time Absolute Error (ITAE), Integral of Absolute Error (IAE), Integral Time Square Error (ITSE). A statistical analysis is carried out here to evaluate the best possible solution. The frequency domain-based loop-shaping method considering the results obtained from various optimization techniques as an initial guess is used for the analytical evaluation of proposed controller parameters. Finally, the robustness of the proposed controllers towards parametric changes in the system is studied and the practical realization of the controllers is analyzed.

The major contribution of this research article is:

i. Estimation and elimination of limit cycle for a system comprising time delays and memory type nonlinearity.
ii. Optimization methods work on minimal error indices for the parameter evaluation of PID and FOPID controllers.
iii. Gain margin and phase margin-based loop shaping method for controller parameter estimation and achieving desired system performance.
iv. Physical realization of non-integer order controllers using Oustaloup recursive filter approximation.

The orientation of this article is as follows: The basic information regarding the fractional-order system is given in section 2. The control problem is mentioned in detail in section 3. The presence of periodic oscillations is examined in section 4. The elimination of the periodic oscillations by using the controllers is presented in section 5. The tests of the robustness of the system towards parameter variations are presented in section 6. While the physical realization of controllers is mentioned in section 7, section 8 includes the final concluding remarks.

2. Preliminary Information

2.1. Non-integral (fractional) calculus

Fractional calculus comprises non-integer order integration and differentiation. The continuous-time integrodifferential operator is demonstrated as [18]:

$$
{}_{\sigma}D_t^{\beta} = \begin{cases} \dfrac{d^{\beta}}{dt^{\beta}}, & \beta > 0 \\ 1, & \beta = 0 \\ \displaystyle\int_{\sigma}^{t} d\tau^{-\beta}, & \beta < 0 \end{cases} \tag{1}
$$

Here, σ and t are the limits of operation, and β is the order of operation. Usually while $\beta \in \mathbb{R}$, but can also be a complex number. The most frequently used definitions for the fractional differential integral operator are as follows: the Grünwald-Letnikov (GL), the Riemann-Liouville (RL), and Caputo expressions. The GL definition of the fractional order derivative of a function g(t) is presented as follows [18]:

$$
{}_{\sigma}D_t^{\beta} g(t) = \lim_{h\to 0} \frac{1}{h^{\beta}} \sum_{j=0}^{\left[\frac{t-\sigma}{h}\right]} (-1)^j \binom{\beta}{j} g(t - jh) \tag{2}
$$

Here $(-1)^j \binom{\beta}{j}$ is the binomial coefficient, $c_j^{(\beta)}$ and h are the differentiation length. The RL definition is expressed as:

$$
{}_{\sigma}D_t^{\beta} g(t) = \frac{1}{\Gamma(n-\beta)} \frac{d^n}{dt^n} \int_{\sigma}^{t} \frac{g(\tau)}{(t-\tau)^{\beta-n+1}} \, d\tau \tag{3}
$$

Here $\Gamma(.)$ is the Euler's Gamma function and n is the order of differentiation. The Caputo definition of fractional order derivatives can be written as:

$$
{}_{\sigma}D_t^{\beta} g(t) = \frac{1}{\Gamma(n-\beta)} \int_{\sigma}^{t} \frac{g^n(\tau)}{(t-\tau)^{\beta-n+1}} \, d\tau \tag{4}
$$

Where $n - 1 < \beta < n$. The Laplace transform method is routinely used for the solution of the engineering problems. The Laplace transform of the RL fractional order derivative is:

$$
\mathcal{L}\left\{{}_0D_t^{\beta} g(t)\right\} = s^{\beta}G(s) - \sum_{k=0}^{n-1} s^k \left[{}_0D_t^{\beta-k-1} g(t)\right] \tag{5}
$$

Similarly, the Laplace transform of Caputo's fractional order derivative is:

$$
\mathcal{L}\left\{{}_0D_t^{\beta} g(t)\right\} = s^{\beta}G(s) - \sum_{k=0}^{n-1} s^{\beta-k-1} f^{(m)}(0) \tag{6}
$$

Now, for zero initial condition (i.e. the assumption generally considered to obtain the transfer function of any systems), the Laplace transform of the fractional order derivative of the order β in GL, RL, and Caputo is reduced to:

$$
\mathcal{L}\left\{{}_0D_t^{\beta} g(t)\right\} = s^{\beta}G(s) \tag{7}
$$

2.2. Non-integer (fractional) order system

The expression of a non-integral order control system considering the non-integral differential equation is given as follows [18,26]:

$$
\begin{aligned} &a_n D^{\alpha_n} c(t) + a_{n-1} D^{\alpha_{n-1}} c(t) + \cdots + a_0 D^{\alpha_0} c(t) = \\ &b_m D^{\beta_m} u(t) + b_{m-1} D^{\beta_{m-1}} u(t) + \cdots + b_0 D^{\beta_0} u(t) \end{aligned} \tag{8}
$$

Here the operator $D^{\gamma} \equiv {}_0D_t^{\beta}$ represents the GL or the RL or Caputo′s non-integral differentiation. The above integrodifferential equation is presented in the Laplace domain as:

$$
\mathcal{L}\left\{\frac{d^n g(t)}{dt^n}\right\} = s^n \mathcal{L}\{g(t)\} - \sum_{i=0}^{m-1} s^k \left[\frac{d^{n-1-i}}{dt^{n-1-i}}\right]\Bigg|_{t=0} \tag{9}
$$

Therefore, with zero initial condition, the non-integer order transfer function is expressed as:

$$
G(s) = \frac{C(s)}{U(s)} = \frac{b_m s^{\beta_m} + b_{m-1} s^{\beta_{m-1}} + \cdots + b_1 s^{\beta_1} + b_0 s^{\beta_0}}{a_n s^{\alpha_n} + a_{n-1} s^{\alpha_{n-1}} + \cdots + a_1 s^{\alpha_1} + a_0 s^{\alpha_0}} \tag{10}
$$

In the above expression α_i(a = 0, 1, 2, …, n), β_i(in = 0, 1, 2, …, m) are real and can be structured as $\alpha_n > \alpha_{n-1} > \cdots > \alpha_0$, and $\beta_m > \beta_{m-1} > \cdots > \beta_0$.

2.3. Realization of non-integer (fractional) order system

The physical realization of the non-integer (fractional) order controllers having non-integer (fractional) order integrators and differentiators is difficult due to infinite memory requirements. Hence some approximations like the Oustaloup method [27], and continued fractional expansion [24,25] are needed during these implementations. The most common approach is the Oustaloup recursive filter approximation method that approximates the fractional order system in the s-domain over a selected lower and upper-frequency range $[\omega_b, \omega_h]$.

Within the frequency range $\omega \in [\omega_b, \omega_h]$, the Oustaloup filter is expressed as [27]:

$$
G_F(s) = s^{\beta} = K \prod_{i=-N}^{N} \frac{s + \omega_i'}{s + \omega_i} \tag{11}
$$

Here, the zero ω_i', the pole ω_i, and the gain K of the system can be evaluated from the following expressions.

$$
\omega_i' = \omega_b \left(\frac{\omega_h}{\omega_b}\right)^{\frac{i+N+0.5(1-\beta)}{2N+1}} \tag{12}
$$

$$
\omega_i = \omega_b \left(\frac{\omega_h}{\omega_b}\right)^{\frac{i+N+0.5(1+\beta)}{2N+1}} \tag{13}
$$

$$
K = \omega_h^{\beta} \tag{14}
$$

While β is the order of fractional differentiation $(\beta > 0)$, *N* is the order of the approximation, and *2N+1* is the order of the Oustaloup filter. Here ω_b is the lower limit and ω_h is the upper limit of the frequency. Usually, $\omega_b.\omega_h = 1$. In this article, the Oustaloup 11th order filter approximation *N=5* in the frequency range of [10^{-3}, 10^{3}] rad/s is considered. The FOMCON toolbox in MATLAB [19,20] along with the function oustafod $(\beta, N, \omega_b, \omega_h)$ is considered for the above realization procedure.

2.4. Describing function (DF) method

The DF method is a frequency domain-based method used to analyze nonlinear systems. It is classified as the ratio of the fundamental output of the system to the applied input sinusoid [1,2]. Numerical values of the DF depend upon the magnitude of input sinusoid *X* and frequency *ω* of the nonlinear dynamical system. Consider a SISO autonomous nonlinear feedback control process as presented in Figure 1 having $u(t) = 0$, describing function $N(X, \omega)$, and the process transfer function $G(s)$.

The steady-state existence of the possible limit cycle is characterized by:

$$1 + N(X, \omega)G(s)|_{s \to j\omega} = 0 \tag{15}$$

i. The Nyquist criterion for the persistence of limit cycle oscillations [1]:

$$\left|\frac{-1}{N(X, \omega)}\right|_{X = X_o} = |G(j\omega)|_{\omega = \omega_o} \tag{16}$$

Here, X_o and ω_o are the corresponding magnitude and frequency of the oscillations. Thereby, the frequency at the intersection of the Nyquist curve of G(s) and negative inverse curve of $[-1/N(X)]$ corresponds the presence of the limit cycle. The behavior of the limit cycle should be stable for a periodic oscillation of constant magnitude and frequency.

ii. The Tsypkin's criterion for a stable limit cycle oscillation [1]: The critical points of $[-1/N(X)]$ plot lie to the left side of the polar plot curve of $G(j\omega)$.

2.5. Concept of backlash nonlinearity

The backlash or gear play is usually found in the mechanical system consisting of gear trains. Although the gear meshes are manufactured for very minimal backlash; but due to friction among the gear teeth, the backlash increases and thereby decreases the system efficiency. Very large value of backlash will produce inappropriate system operation. Backlash can cause undesirable oscillations in the feedback control loop. The DF method can be used to analyze the effect of backlash nonlinearity in the nonlinear control system. The DF expression of backlash nonlinearity is presented as [2,3]:

$$N(X) = \begin{cases} 0, & X < H \\ \frac{k}{\pi}\left[\left(\frac{\pi}{2} + \beta + 0.5\sin(2\beta)\right) - j\cos^2\beta\right], & X \geq H \end{cases} \tag{17}$$

Where $\beta = \sin^{-1}\left(1 - \frac{2H}{X}\right)$.

Let us consider the backlash parameters to be k = 1 and H = 0.05. By separating the real and imaginary terms, the above equation can be presented in its magnitude and phase angle form as follows:

$$|N(X)| = \frac{k}{\pi}\sqrt{\left(\frac{\pi}{2} + \beta + 0.5\sin(2\beta)\right)^2 + \cos^4\beta} \tag{18}$$

$$\angle N(X) = -\tan^{-1}\left(\frac{\cos^2\beta}{\frac{\pi}{2} + \beta + 0.5\sin(2\beta)}\right) \tag{19}$$

Now, the analytical calculation of limit cycle parameters can be carried out by using (18) and (19) as described below.

3. Control Problem Formulation

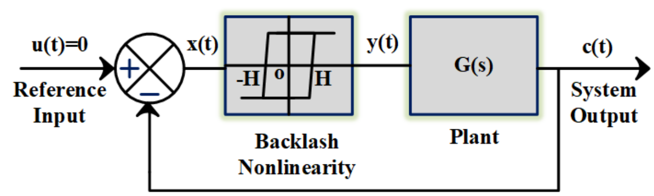

Fig. 1. A feedback control system with backlash nonlinearity

A nonlinear feedback control system presented in Figure 1 includes a DC motor plant and memory-type backlash nonlinearity. The existence of a periodic oscillation is examined for the given system in the presence of a delay time. The plant in Figure 1 is a DC motor servo utilized for position control applications [2,3]. Here the contacting gears of the gear train produce backlash nonlinearity in the system.

The transfer function of the plant in Figure 2 can be found by considering the shaft angular displacement $\theta_L(s)$ as output variable and applied armature voltage $E_A(s)$ as the input variable and converting the feedback gain as unity [2,3] as mentioned in Figure 3. The effect of gear ratio, backlash, and time delay is also taken into consideration during the estimation of the transfer function.

$$G(s) = \frac{\theta_L(s)}{E_A(s)} \tag{20}$$
$$= \frac{nK_AK_{PO}K_T\ e^{-Ls}}{s[s^2(JL_A) + s(BL_A + JR_A) + (BR_A + K_TK_B)]}$$

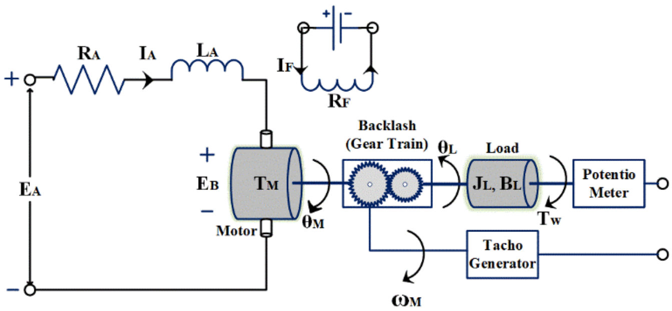

Fig. 2. An armature voltage-controlled DC servo motor

Table 1. Parameter values of the system [2,3]

Parameters	Representation	Value	Unit
$\mathbf{R_A}$	Armature Winding Resistance	10	Ohm
$\mathbf{L_A}$	Armature Winding Inductance	0.1	Henry
$\mathbf{K_A}$	Amplification Gain	1	-
$\mathbf{K_B}$	Back EMF Constant	1	Volt/(rad/s)
$\mathbf{K_T}$	Motor Torque Constant	0.8	Volt/(rad/s)
$\mathbf{K_{PO}}$	Potentiometer Sensitivity	1.5	Volt/rad
J	Inertia Constant	2.025	N-m/(rad/s2)
B	Viscous frictional Coefficient	0.0025	N-m/(rad/s)
n	Gear Ratio	0.5	-

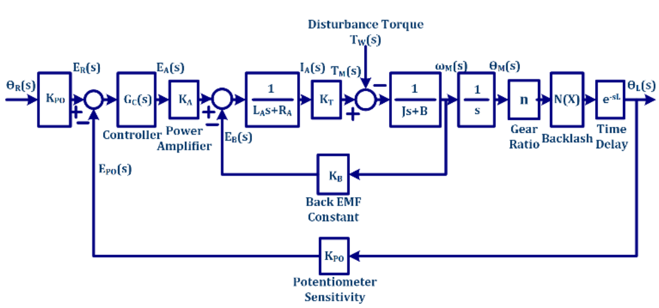

Fig. 3. Block Diagram of the DC motor with Backlash

By using values of the parameters from Table 1 along with a time delay of L= 0.01 s, the equation (20) could be simplified as:

$$G(s) = \frac{0.6}{s[s^2(0.2025) + s(20.2522) + 1.0250]} e^{-0.01s} \tag{21}$$

Assuming $s = j\omega$ for the analysis in the frequency domain, the function $G(j\omega)$ can be presented as mentioned below.

$$G(j\omega) = \frac{0.6 \ e^{-0.01(j\omega)}}{(j\omega)[(j\omega)^2(0.2025) + (j\omega)(20.2522) + 1.0250]} \tag{22}$$

The above equation can be simplified and separated into magnitude and phase angle parts as follows:

$$|G(j\omega)| = \frac{0.6}{\sqrt{(20.2522\omega^2)^2 + (0.2025\omega^3 - 1.025\omega)^2}} \tag{23}$$

$$\angle G(j\omega) = -\tan^{-1}\left(\frac{0.2025\omega^3 - 1.025\omega}{20.2522\omega^2}\right) - (0.01\omega) \tag{24}$$

The performance above the DC motor model in the presence of backlash and time delays is evaluated in this article. The above system with backlash nonlinearity is checked for any possible existence of limit cycle oscillations as presented in the next section.

4. Limit Cycle Prediction

An analytical evaluation of the periodic limit cycle oscillations can also be carried out by using (15) as:

$$N(X,\omega)G(s)|_{s=j\omega} = -1 = 1\angle\pi \tag{25}$$

It emphasizes the following relationships:

i. The closed-loop amplitude gain criterion:

$$|N(X_o,\omega_o)G(j\omega_o)| = 1 \tag{26}$$

ii. The closed-loop phase angle criterion:

$$\angle N(X_o,\omega_o) + \angle G(j\omega_o) = \pi \tag{27}$$

Analytical solutions of (26) and (27) produces particulars about the limit cycle magnitude X_o and the frequency ω_o.

4.1. Analytical method

The analytical evaluation procedure involves the solution of the closed-loop magnitude and phase angle condition for the prediction of periodic limit cycle oscillations. The closed-loop gain condition (26) leads to the following equation:

$$\frac{\left(\frac{0.6}{\pi}\right)\sqrt{\left(\frac{\pi}{2} + \beta + 0.5\sin(2\beta)\right)^2 + \cos^4\beta}}{\sqrt{(20.2522\omega^2)^2 + (0.2025\omega^3 - 1.025\omega)^2}} = 1 \tag{28}$$

This gives:

$$\left(\frac{0.6}{\pi}\right)^2\left\{\left(\frac{\pi}{2} + \beta + 0.5\sin(2\beta)\right)^2 + \cos^4\beta\right\} = (20.2522\omega^2)^2 + (0.2025\omega^3 - 1.025\omega)^2 \tag{29}$$

The above equation can be simplified as:

$$\frac{0.36}{\pi^2}\left\{\left(\frac{\pi}{2} + \beta + 0.5\sin(2\beta)\right)^2 + \cos^4\beta\right\} - \{(20.2522\omega^2)^2 + (0.2025\omega^3 - 1.025\omega)^2\} = 0 \tag{30}$$

The close loop phase condition (22) produces:

$$-\tan^{-1}\left(\frac{0.2025\omega^3-1.025\omega}{20.2522\omega^2}\right)-\tan^{-1}\left(\frac{\cos^2\beta}{\frac{\pi}{2}+\beta+0.5\sin(2\beta)}\right)-0.01\omega=\pi \quad (31)$$

This provides:

$$\tan^{-1}\left(\frac{0.2025\omega^3-1.025\omega}{20.2522\omega^2}\right)+\tan^{-1}\left(\frac{\cos^2\beta}{\frac{\pi}{2}+\beta+0.5\sin(2\beta)}\right)=-\pi-0.01\omega \quad (32)$$

As,

$$\tan^{-1}(x)+\tan^{-1}(y)=\tan^{-1}\left(\frac{x+y}{1-xy}\right) \quad (33)$$

The above expression is simplified as:

$$\left[\frac{\left(\frac{\pi}{2}+\beta+0.5\sin(2\beta)\right)(0.2025\omega^3-1.025\omega)+\cos^2\beta(20.2522\omega^2)}{\left(\frac{\pi}{2}+\beta+0.5\sin(2\beta)\right)(20.2522\omega^2)-\cos^2\beta(0.2025\omega^3-1.025\omega)}\right]=-\tan(0.01\omega) \quad (34)$$

As the equations (30), and (34) are nonlinear, these could be solved by using the MATLAB fsolve() function assuming an initial guess of [1,1]. The solution thus obtained is $X_o=0.1794$ and $\omega_o=0.1512$ rad/s and is provided in Table 2 for further comparison with alternate methods.

4.2. Graphical method

A graphical evaluation of the periodic oscillations could be obtained using the superimposed Nyquist plot of G(s) along with the negative inverse plot of $[-1/N(X)]$. The possible intersection of both curves suggests the presence of periodic oscillations. The behavior of the limit cycle must be stable to have a sustained periodic oscillation of constant amplitude and frequency. It could similarly be derived from (16) as follows:

$$\left|\frac{-1}{N(X)}\right|_{X=X_o}=|G(j\omega)|_{\omega=\omega_o} \quad (35)$$

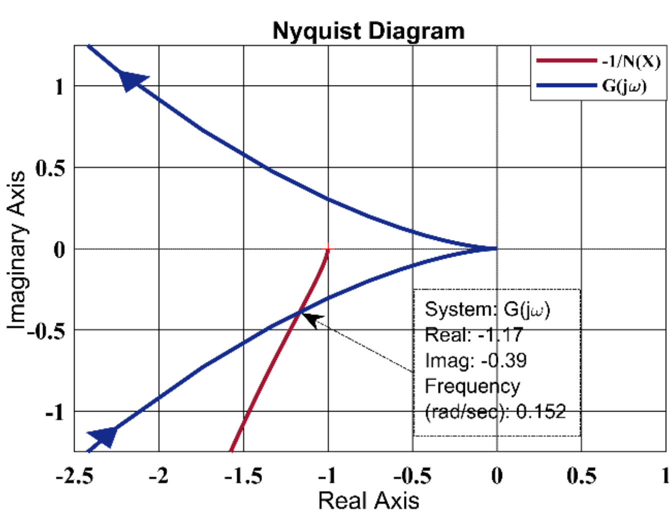

Fig. 4. Superimposed Nyquist plot of G(jω) with negative inverse plot of N(X) for backlash.

The overlapped Nyquist plot and the negative inverse graph of $[-1/N(X)]$ are presented in Figure 4, which signifies the possible solutions and the existence of limit cycle. The value of oscillation frequency $\omega_o=0.152$ rad/s is interpreted from the intersection point and the oscillation amplitude is obtained from (35) as per the following procedure.

It is evident from Figure 4 that:

$$G(j\omega_o)=-1.17-j0.39 \quad (36)$$

$$\Longrightarrow |G(j\omega_o)|=\sqrt{(1.17)^2+(0.39)^2}=1.2332 \quad (37)$$

Again, as per close loop gain condition (26):

$$|G(j\omega_o)N(X_o)|=1$$

$$\Longrightarrow |N(X_o)|=\frac{1}{|G(j\omega_o)|}=\frac{1}{1.2332}=0.8108 \quad (38)$$

By considering the value of $|N(X_o)|$ from equation (18) in the above equation, we get:

$$\frac{1}{\pi}\sqrt{\left(\frac{\pi}{2}+\beta+0.5\sin(2\beta)\right)^2+\cos^4\beta}=0.8108 \quad (39)$$

As, $\beta=1-\frac{2H}{X_o}$,

Assuming an initial guess of $X_o=0.1$, the above equation (39) can be simplified using the fsolve() function of MATLAB that evaluates the value of $X_o=0.1774$ as mentioned in Table 2. The above results of the limit cycle can be examined by performing simulations.

4.3. Digital simulations

The simulation output for the nonlinear system in Figure 1 is presented in Figure 5 which validates the presence of periodic oscillations. Observations from Table 2 indicate that the amplitude and frequency of the oscillations are similar in all the methods.

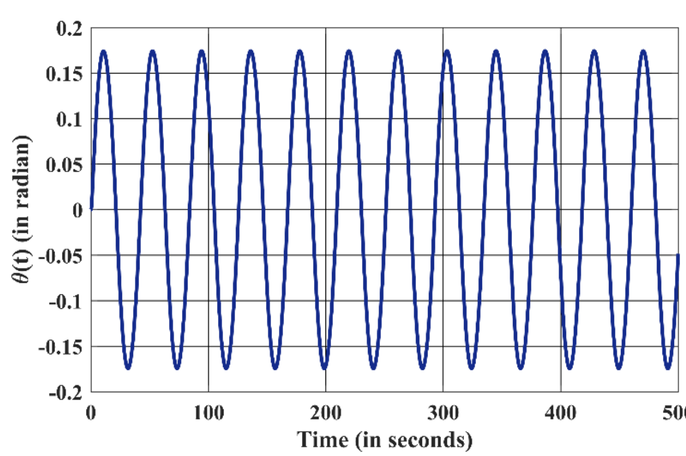

Fig. 5. Zero input response of a plant with backlash

Table 2. Comparison of Limit cycle parameters obtained by different methods

Backlash Nonlinearity	Limit Cycle Amplitude X_o	Limit Cycle Frequency ω_o (rad/s)
Analytical Method	0.1794	0.1512
Graphical Method	0.1774	0.1520
Digital Simulation	0.1770	0.1510

Although the evaluation of the limit cycle is done with the zero-input response, its effect can also be noticed in the step response of the plant as seen in Fig. 6. The output response of the system exhibiting a limit cycle can be presented mathematically as follows:

$$c(t) = -e(t) = -X_o \sin[\omega_o(t - L)] \tag{40}$$

This gives:

$$c(t) = -0.1770 \ \ \sin(0.1510t - 0.0151) \tag{41}$$

4.4. Effect of parameter variations

The variations in magnitude and frequency of periodic oscillations due to the parameter variations such as changes in delay times and backlash magnitudes are discussed as follows.

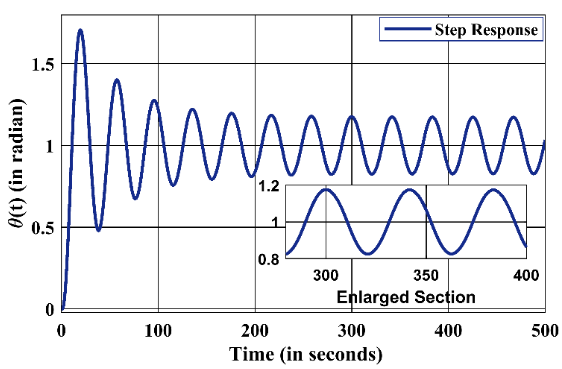

Fig. 6. Step response of the plant with backlash

4.4.1. Variations in Delay Time

Physical dynamical systems commonly encounter time delays whose magnitude increases with enhancement in the complexity of the system. The existence of a large delay time is a prime cause of loss of stability and deviations in system performance.

Table 3. Limit cycle parameters under different time delays

Parameters	Time Delay L (in seconds)		
	$L = 0.01s$	$L = 0.1s$	$L = 0.5s$
Amplitude of Limit Cycle Oscillation X_o	0.1770	0.1830	0.2500
Frequency of Limit Cycle Oscillation ω_o (rad/s)	0.1510	0.1511	0.1563

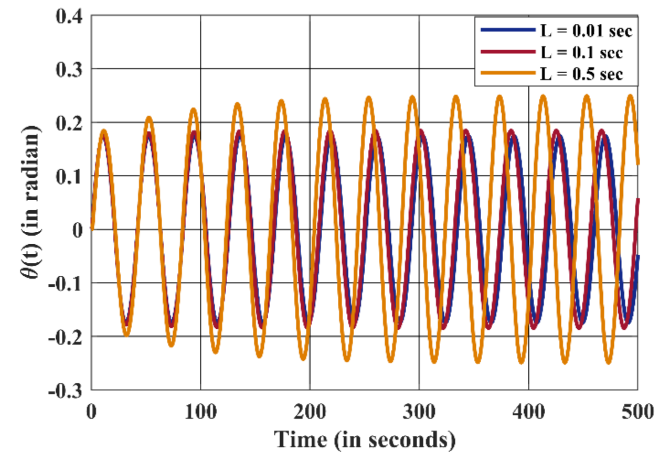

Fig. 7. Zero input response of the system with various time delays

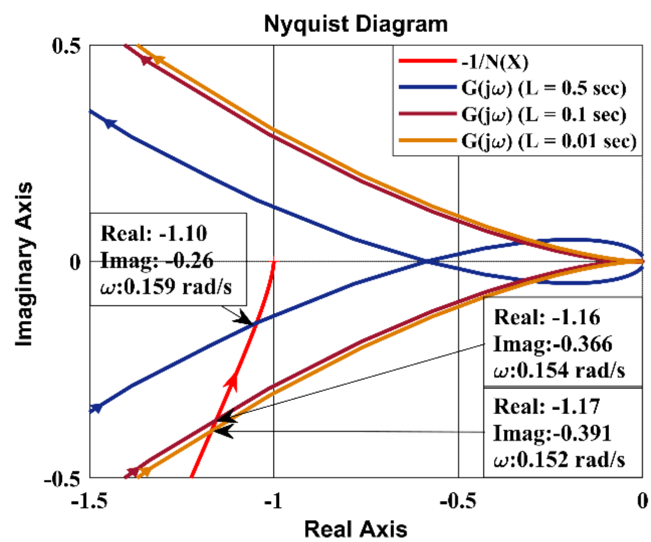

Fig. 8. Superimposed Nyquist plot of G(jω) and negative inverse plot of N(X) under variations in time delays

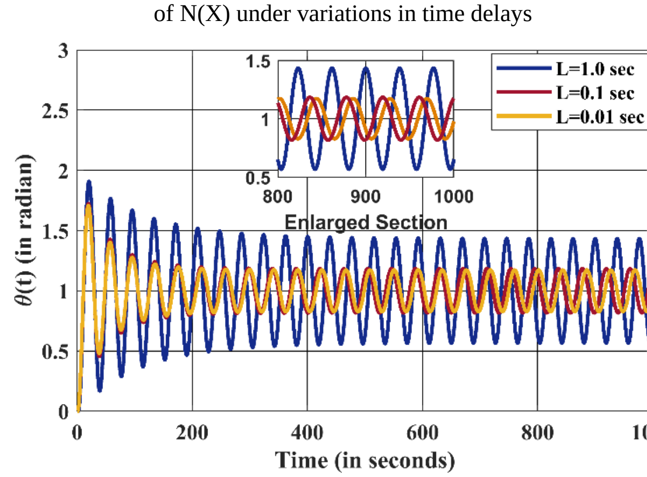

Fig. 9. Step response of the system under variations in time delays

Let the plant in Figure 1 have different time delays. Studies from Table 3 reveal an increment in oscillation magnitude with a corresponding increase in time delays whereas the frequency mostly remains unaltered as shown in Figure 7. Its similar phasor diagram-based interpretation is provided in Figure 8. The step response of the system of Figure1 under various time delays is shown in Figure 9.

4.4.2. Variations in backlash amplitude

The existence of backlash in mechanical systems causes sustained periodic oscillations. These limit cycle oscillations will aggregate the mechanical wear of the system and thereby further enhance the backlash. Variations in the backlash amplitude may vary the oscillation behavior of the nonlinear system. The information from Table 4 suggests an increase in oscillation amplitude for an increase in the dead band, even if the oscillation frequency remains the same as found in Figure 10. Its similar phasor diagram-based analysis is shown in Figure 11. Likewise, the step response of the system mentioned in Figure 1 under different backlash amplitudes is shown in Figure 12.

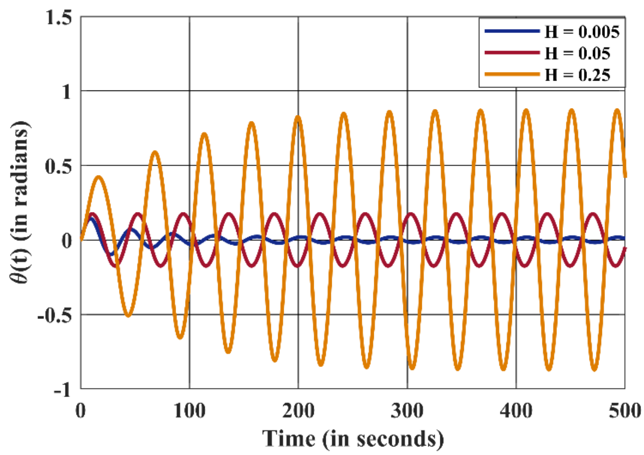

Fig. 10. Zero input response of the system under variations in backlash magnitude

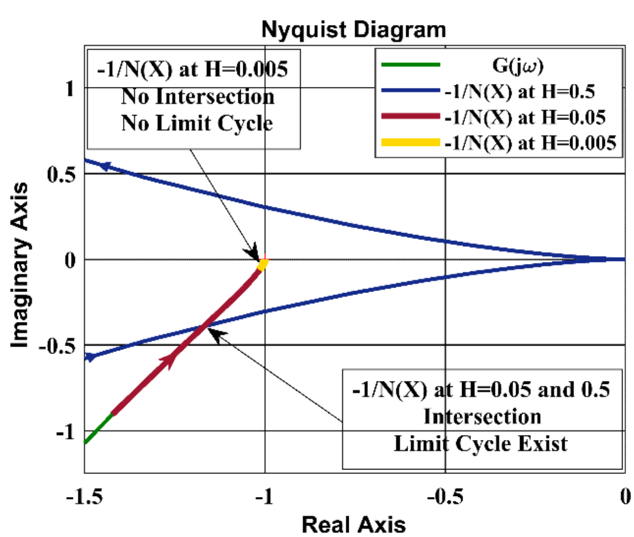

Fig. 11. Superimposed Nyquist plot of G(jω) and negative inverse plot of N(X) under variations in backlash

Table 4. Limit cycle under different backlash amplitudes

Parameters	Dead Band Width (H)		
	$H = 0.005$	$H = 0.05$	$H = 0.25$
Amplitude of Limit Cycle Oscillation X_o	0.0180	0.1770	0.8730
Frequency of Limit Cycle Oscillation ω_o (rad/s)	0.1456	0.1510	0.1513

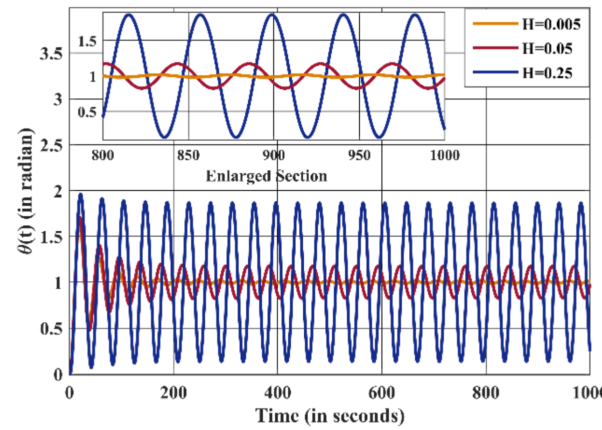

Fig. 12. Step response of the system under variations in backlash magnitude

5. Limit Cycle Elimination

The periodic oscillations present in the system of Figure 1 due to backlash nonlinearity create inaccuracy in the required position control problems.

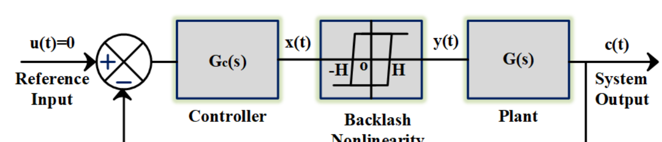

Fig. 13. A feedback control system with controller and backlash

Controllers are designed to address the transient and steady-state inaccuracy inherited in the system dynamics. The plant of Figure 1 with a desired controller is presented in Figure 13 for further analysis. A classical integer order PID controller is expressed by the below-mentioned transfer function:

$$G_C(s) = K_P + \frac{K_I}{s} + K_D s \tag{42}$$

Here, K_P denotes the proportional gain, K_I denotes the integration coefficient, and K_D denotes the derivative coefficient. Optimal values of K_P, K_I, K_D could provide desired control efforts based on reference tracking and rejecting disturbances. Substituting $s = j\omega$ for the analysis in the frequency domain, the transfer function $G_{C\_PID}(j\omega)$ can be expressed as follows.

$$G_C(j\omega) = K_P + \frac{K_I}{j\omega} + jK_D\omega = K_P + j\left(K_D\omega - \frac{K_I}{\omega}\right) \quad (43)$$

The amplitude and phase of the PID controller is given as:

$$|G_C(j\omega)| = \sqrt{{K_P}^2 + \left(K_D\omega - \frac{K_I}{\omega}\right)^2} \quad (44)$$

$$\angle G_C(j\omega) = \tan^{-1}\left(\frac{K_D\omega^2 - K_I}{\omega K_P}\right) \quad (45)$$

Further, the FOPID controller is presented in the Laplace domain as mentioned below.

$$G_C(s) = K_P + \frac{K_I}{s^\lambda} + K_D s^\mu, \qquad \lambda, \mu > 0 \quad (46)$$

While, λ denotes the integrator order, and μ is the differentiator order. The similarity between the PID and FOPID is established when λ=1 and μ=1. Further, substituting $s = j\omega$ for analysis in the frequency domain, we have:

$$G_C(j\omega) = K_P + \frac{K_I}{\omega^\lambda} j^{-\lambda} + K_D\omega^\mu j^\mu \quad (47)$$

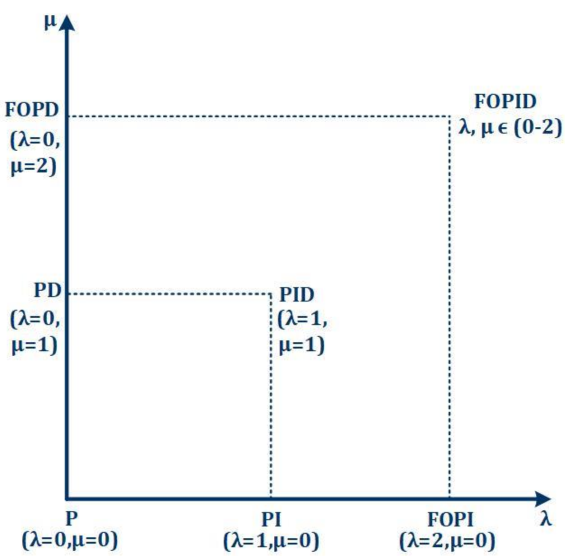

Fig. 14. 2-D plane representation of $PI^\lambda D^\mu$ Controllers [38]

Now using De-Moivre's theorem, we get [31]:

$$(z)^n = |z|^n(\cos n\theta + j\sin n\theta) \quad (48)$$

For, $z = j \;\Rightarrow\; |z| = 1, \theta = \frac{\pi}{2}$.

Hence, we find:

$$j^\mu = \cos\frac{\mu\pi}{2} + j\sin\frac{\mu\pi}{2} \text{ and } j^{-\lambda} = \cos\frac{\lambda\pi}{2} - j\sin\frac{\lambda\pi}{2} \quad (49)$$

Therefore, the above equation becomes:

$$G_C(j\omega) = K_P + \frac{K_I}{\omega^\lambda}\left(\cos\frac{\lambda\pi}{2} - j\sin\frac{\lambda\pi}{2}\right) + K_D\omega^\mu\left(\cos\frac{\mu\pi}{2} + j\sin\frac{\mu\pi}{2}\right) \quad (50)$$

Now separating the magnitude and phase part we have:

$$|G_C(j\omega)| = \sqrt{\left(K_P + \frac{K_I}{\omega^\lambda}\cos\frac{\lambda\pi}{2} + K_D\omega^\mu\cos\frac{\mu\pi}{2}\right)^2 + \left(K_D\omega^\mu\sin\frac{\mu\pi}{2} - \frac{K_I}{\omega^\lambda}\sin\frac{\lambda\pi}{2}\right)^2} \quad (51)$$

$$\angle G_C(j\omega) = \tan^{-1}\left(\frac{K_D\omega^\mu\sin\frac{\mu\pi}{2} - \frac{K_I}{\omega^\lambda}\sin\frac{\lambda\pi}{2}}{K_P + \frac{K_I}{\omega^\lambda}\cos\frac{\lambda\pi}{2} + K_D\omega^\mu\cos\frac{\mu\pi}{2}}\right) \quad (52)$$

The optimal tuning of integer and fractional order controllers for the quenching of limit cycle is discussed below. There exist various methods for the evaluation of parameters of controllers. While some of them are stochastic optimization-based procedures, others are deterministic approaches. Both possess their own advantages and disadvantages as mentioned below.

5.1. Optimization techniques for parameter tuning

Metaheuristic algorithms operate on an approximate structural model and hence could provide befitting solutions to real-world problems [38-41]. Varieties of optimization techniques are present in literature classified as Evolutionary algorithms, Swarm based algorithms, Physics-based algorithms, and some other population-based algorithms, etc. Hence, it is difficult to adopt a specific algorithm for the solution of a specific problem. Therefore, a comparison is been made between some recent optimization techniques like ALO, PSO, GWO, WOA, and MFO based on the minimization of error indices to find the optimal parameters of the controllers. Let the error function be $e(t)$, and the time variable is t; then, some of the common cost functions are provided below [38-41].

i. The ISE objective function

$$J = \int_0^{t_{sim}} e^2(t)\; dt \quad (53)$$

ii. The IAE objective function

$$J = \int_0^{t_{sim}} |e(t)|\; dt \quad (54)$$

iii. The ITSE objective function

$$J = \int_0^{t_{sim}} te^2(t)\; dt \quad (55)$$

iv. The ITAE objective function

$$J = \int_0^{t_{sim}} t|e(t)|\; dt \quad (56)$$

Along with the above error-based cost functions, this paper also tests a time specification-based objective function (ZLG) as proposed by Zwe-Lee Gaing [47]. Here, β is the weighting factor whose usual values lie within [0.7-1.5]. Further, M_P denotes the peak overshoot, E_{SS} denotes the error at steady state, T_R denotes the rise time, and T_S denotes the settling time respectively. It is worth mentioning here that while $\beta > 0.7$ suppresses the overshoot and steady-state error; $\beta < 0.7$ decreases the T_R and T_S. In this article, the best system response is found for $\beta = 1.5$.

v. The ZLG objective function

$$J = \left(1 - e^{-\beta}\right).\left(M_P + E_{SS}\right) + \left(e^{-\beta}\right).\left(T_S - T_R\right) \tag{57}$$

The above objective functions can be used alone or in combination to debug the optimal values of the controller.

Table 5. Parametric values for optimization methods

Optimization Techniques	Parameter Settings
ALO	Maximum Iterations = 100 No of Search Agents = PID (30), PIλDμ (30)
PSO	Maximum Iterations = 100 Total Population = PID (30), PIλDμ (30) Inertial weight = 1 Damping Ratio =0.99 Learning Index (personal) = 1.5 Learning Index (global) = 2.0
GWO	Maximum Iterations = 100 No of Search Agents = PID (30), PIλDμ (30)
WOA	Maximum Iterations = 100 No of Search Agents = PID (30), PIλDμ (30)
MFO	Maximum Iterations = 100 No of Search Agents = PID (30), PIλDμ (30)

The parametric settings for the optimization techniques during this error function minimization procedure are mentioned in Table. 5. In any optimization process, the search region, number of search agents, and number of iterations are vital to draw a precise conclusion. The choice of the search range is usually a hit-and-trial procedure. Simulations usually encounter problems like not a number (NAN), saturation to upper limit etc. during this procedure. Further, the choices for the number of iterations and the number of search agents are usually a trade-off between preciseness and simulation time.

5.1.1. Parameter estimation of PID controllers

The nonlinear feedback loop of Figure 13 considering a PID controller is optimized using different optimization methods within the parameter range $K_P \in [0,75]$, $K_P \in [0,75]$, and $K_P \in [0,75]$. This article considers the above objective functions and carries out a statistical study emphasizing least value of the mean, standard deviation, maximum, and minimum values of cost functions.

The cost function that produces the least mean value is considered the best-performing objective function under specified system parameters. The statistical analysis is carried out with techniques like ALO, PSO, GWO, WOA, and MFO considering the parameters as mentioned in Table 5. The values of different cost functions are obtained by engaging 30 search agents for 100 iterations with 10-time repetitions and are presented in Table 6. As the optimization algorithms are stochastic, therefore an appropriate statistical study can lead to a proper performance-oriented conclusion.

Table 6. Statistical analysis considering PID controllers

Cost Functions		Optimization Methods				
		ALO	PSO	GWO	WOA	MFO
ISE	Mean	0.6074	0.6074	0.6074	0.6799	**0.6073**
	Std. Dev.	7.53 E-06	5.72 E-06	1.03 E-05	8.5 2E-06	5.52 E-06
	Max.	0.6074	0.6074	0.6074	0.6799	0.6074
	Min.	0.6074	0.6074	0.6074	0.6799	0.6074
IAE	Mean	**0.9816**	1.3475	0.9909	0.9908	0.9885
	Std. Dev.	0.0016	0.2761	0.0023	0.0008	0.0037
	Max.	0.9853	1.5475	0.9922	0.9914	0.9912
	Min.	0.9792	0.9799	0.9812	0.9882	0.9797
ITSE	Mean	0.8735	0.8735	0.8735	0.8735	**0.8734**
	Std. Dev.	2.47 E-05	4.70 E-05	2.52 E-05	2.55 E-05	1.84 E-05
	Max.	0.8735	0.8736	0.8736	0.8735	0.8735
	Min.	0.8734	0.8735	0.8735	0.8734	0.8734
ITAE	Mean	**1.8937**	5.2995	2.0771	2.0671	2.2065
	Std. Dev.	0.0858	0.0343	0.1092	0.1455	0.0809
	Max.	2.2304	5.3487	2.2431	2.2573	2.3024
	Min.	1.8172	5.2469	1.9077	1.785	2.0053
ZLG	Mean	0.2154	0.7773	0.1993	0.1997	**0.1991**
	Std. Dev.	0.0237	0.4871	0.0001	0.0013	2.75 E-05
	Max.	0.2632	1.1547	0.1996	0.2033	0.1991
	Min.	0.1991	0.1992	0.1992	0.1991	0.1991

Table 7. PID parameters obtained against best cost functions

Cost Functions		K_P	K_I	K_D	T_R	T_S	M_P	E_{SS}
ISE	0.6074	75	0	56.228	1.175	3.885	11.285	0.00036
IAE	0.9792	74.916	0.019	69.097	1.402	3.930	4.446	0.00037
ITSE	0.8734	75	0	60.409	1.240	3.934	8.698	-0.00067
ITAE	1.8172	72.69	0	74.997	1.584	3.446	2.026	-0.00005
ZLG	0.1991	72.56	0	75	1.587	3.447	2.022	0.00002

It is noticed from Table 6 that the least mean values of objective functions are obtained for ISE with MFO, IAE with ALO, ITSE with MFO, and ITAE with ALO. For the minimum values of the cost functions, the corresponding values of PID are presented in Table 7. A comparison of zero input response and step response for the above plant is provided in Figure 15 and Figure 16 respectively. The result thus obtained by adopting a minimal ITAE index shows better transient performance. It is obvious that due to the existence of periodic oscillations, the controller cannot have an integral component as an integrator emphasizes oscillations in the plant.

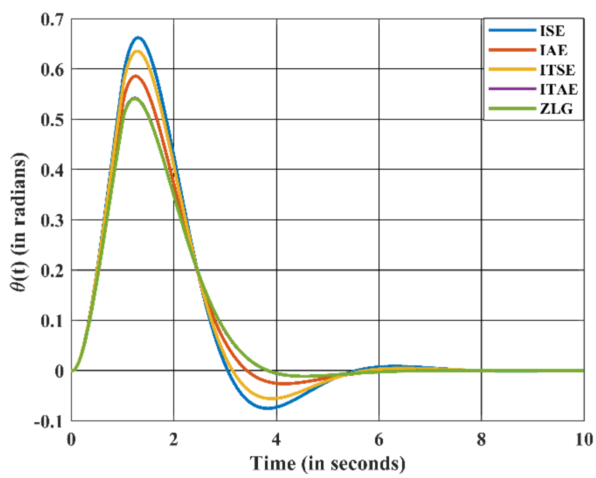

Fig. 15. Zero input response with PID and backlash nonlinearity

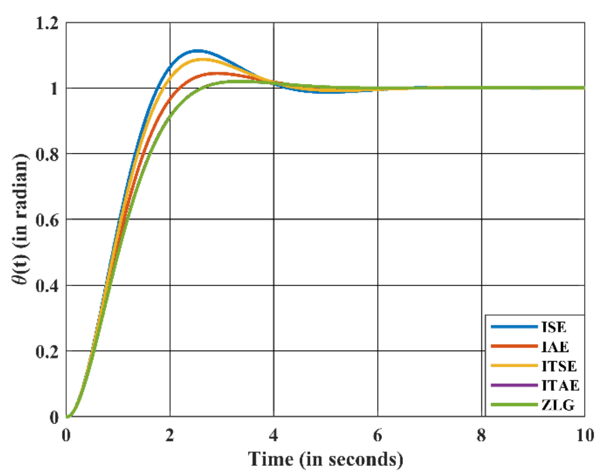

Fig. 16. Step response with PID and backlash nonlinearity

Therefore, the required PID controller towards the elimination of the limit cycle is a PD controller and is expressed as:

$$G_C(s) = 72.69 + 74.997\ s \tag{58}$$

5.1.2. Parameter estimation of $PI^{\lambda}D^{\mu}$ Controllers

The DC motor system of Figure 13 with a $PI^{\lambda}D^{\mu}$ is optimized considering various integral and absolute errors within the same parametric range $K_P \in [0,75]$, $K_I \in [0,75]$, and $K_D \in [0,75]$. Here the values of the fractional exponents are varied over the ranges $\lambda \in [0,1]$, and $\mu \in [0,1]$, as well as $\lambda \in [0,2]$, and $\mu \in [0,2]$. A similar statistical test is performed with the algorithms ALO, PSO, GWO, WOA, and MFO adopting the same parameters as mentioned in Table 5. The solutions thus obtained by engaging 30 search agents with 100 iterations and 10-time such repetitions are provided in Table 8 and Table 9. The optimal values of FOPID controllers selected based on performances are presented in Table 10. The zero and step input responses of the system are compared against various objective functions shown in Figure 17 and Figure 18 respectively indicating superior transient performance for the ITSE index within the range $\lambda \in [0,1]$, and $\mu \in [0,1]$.

It is observed from Figure 17 and Figure 18 that the parametric setting of $\lambda \in [0,2]$, and $\mu \in [0,2]$ show poor transient characteristics in terms of M_P and marginal T_S than the parametric setting of $\lambda \in [0,1]$, and $\mu \in [0,1]$. Therefore, considering the minimal ISTE cost function within a parametric range $\lambda \in [0,1]$, and $\mu \in [0,1]$, the required FOPID controller for the quenching of the limit cycle is expressed as:

$$G_C(s) = 3.8581 + \frac{0.6937}{s^{0.0058}} + 75\ s^{0.9998} \tag{59}$$

Table 8. Statistical analysis considering FOPID controllers

Cost Functions (J_{min})		$PI^{\lambda}D^{\mu}$ Controller ($\lambda \in [0,1], \mu \in [0,1]$)				
		ALO	**PSO**	**GWO**	**WOA**	**MFO**
ISE	Mean	0.23293	0.23250	0.23253	0.23268	**0.23250**
	Std. Dev.	0.00073	0.00010	2.1026 E-05	0.00060	8.3376 E-05
	Max.	0.2347	0.2327	0.2326	0.23518	0.23255
	Min.	0.23247	0.2324	0.23248	0.23223	0.23223
IAE	Mean	0.61229	0.61173	0.60968	0.60853	**0.60443**
	Std. Dev.	0.00725	0.00541	0.00676	0.00670	0.00129
	Max.	0.62477	0.6243	0.62315	0.62175	0.60631
	Min.	0.60523	0.6045	0.60398	0.60192	0.60163
ITSE	Mean	0.32443	0.32279	0.31013	0.31335	**0.30479**
	Std. Dev.	0.00196	0.00082	0.01529	0.01383	0.01586
	Max.	0.32966	0.3234	0.32344	0.32324	0.32324
	Min.	0.32258	0.3207	0.28845	0.28864	0.28844
ITAE	Mean	1.7071	1.89208	1.69853	1.71911	**1.60809**
	Std. Dev.	0.11917	0.21919	0.10666	0.20317	0.10461
	Max.	2.0043	2.2039	1.8389	2.1165	1.7671
	Min.	1.5592	1.3471	1.5221	1.4136	1.4375
ZLG	Mean	0.55189	0.60352	0.15844	0.27093	**0.09789**
	Std. Dev.	0.23883	0.17702	0.17470	0.26908	0.00554
	Max.	0.67583	0.6747	0.65552	0.67199	0.10352
	Min.	0.09594	0.1	0.09207	0.10169	0.09006

Further, a comparative analysis is done between the optimal PID and optimal FOPID and is presented in Figure 19. It can be noticed that the fractional controllers perform better in comparison with their integer counterparts.

Table 9. Statistical analysis considering FOPID controllers

Cost Functions (J_{min})		$PI^{\lambda}D^{\mu}$ Controller ($\lambda \in [0,2], \mu \in [0,2]$)				
		ALO	**PSO**	**GWO**	**WOA**	**MFO**
ISE	Mean	0.16229	0.15814	0.16050	0.16326	0.15440
	Std. Dev.	0.00611	0.00662	0.00740	0.00709	2.23 E-06
	Max.	0.17278	0.16933	0.16942	0.1695	0.15441
	Min.	0.15438	0.15441	0.15438	0.15441	0.1544
IAE	Mean	0.57858	0.58235	0.56347	0.58294	0.56499
	Std. Dev.	0.02604	0.01699	0.03909	0.01962	0.00025
	Max.	0.62044	0.61536	0.60658	0.60865	0.56535
	Min.	0.48457	0.57152	0.56531	0.56484	0.56465
ITSE	Mean	0.27204	0.26788	0.26465	0.27260	0.26090
	Std. Dev.	0.01034	0.01038	0.00853	0.01139	2.28 E-05
	Max.	0.2969	0.28456	0.28457	0.28752	0.26092
	Min.	0.26088	0.26088	0.2609	0.26092	0.26087
ITAE	Mean	1.34348	1.33042	1.28139	1.3729	1.24172
	Std. Dev.	0.07395	0.05918	0.05315	0.19165	0.00824
	Max.	1.4605	1.4329	1.427	2.1237	1.2528
	Min.	1.2239	1.2446	1.2397	1.2361	1.2216
ZLG	Mean	0.50446	0.66605	0.38165	0.33646	0.09875
	Std. Dev.	0.27579	0.01057	0.29417	0.29478	0.00656
	Max.	0.71097	0.6845	0.67198	0.72077	0.1035
	Min.	0.09615	0.6548	0.09575	0.1011	0.08901

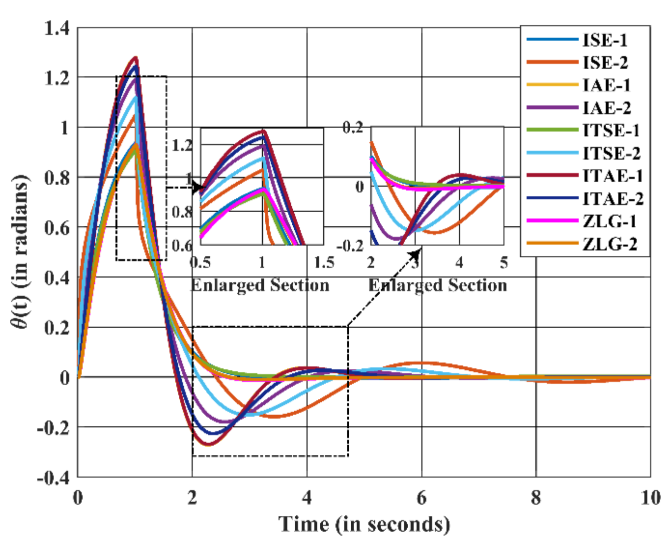

Fig. 17. Zero input response with FOPID and backlash nonlinearity

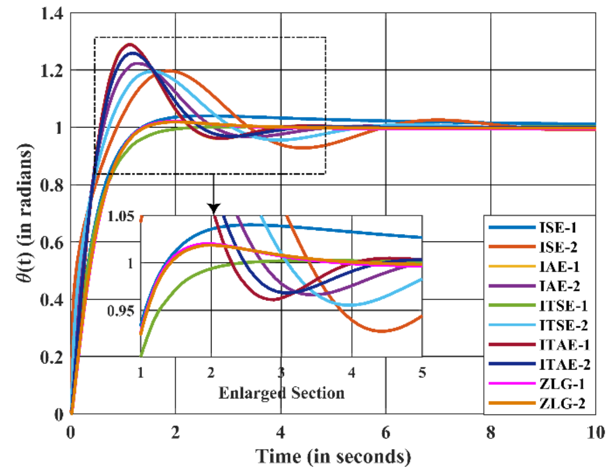

Fig. 18. Step response with FOPID and backlash nonlinearity

Table 10. FOPID parameters obtained against best cost functions

J_{min}	K_P	K_I	K_D	λ	μ	T_R	T_S	M_P	E_{SS}
ISE-1 $\lambda \in [0,1]$, $\mu \in [0,1]$	13.32	0	75	0.604	0.999	0.816	6.578	4.006	0.011
ISE-2 $\lambda \in [0,2]$, $\mu \in [0,2]$	75	75	75	0	1.512	0.639	7.549	19.65	0.007
IAE-1 $\lambda \in [0,1]$, $\mu \in [0,1]$	73.68	75	74.95	0	1	0.419	3.435	28.94	0.0003
IAE-2 $\lambda \in [0,2]$, $\mu \in [0,2]$	74.69	75	74.99	0	1.172	0.460	4.137	22.27	7.7 E-5
ITSE-1 $\lambda \in [0,1]$, $\mu \in [0,1]$	**3.85**	**0.69**	75	**0.005**	**0.999**	**0.924**	1.614	**0.246**	**0.001**
ITSE-2 $\lambda \in [0,2]$, $\mu \in [0,2]$	75	75	75	4.31 E-9	1.332	0.530	4.914	19.48	0.0005
ITAE-1 $\lambda \in [0,1]$, $\mu \in [0,1]$	73.09	74.5	74.97	0	1	0.420	3.442	28.81	0.0003
ITAE-2 $\lambda \in [0,2]$, $\mu \in [0,2]$	67.64	75	75	0	1.047	0.438	3.630	25.85	0.0001
ZLG-1 $\lambda \in [0,1]$, $\mu \in [0,1]$	1.11	0	75	0.993	0.886	0.830	2.022	2.024	0.0049
ZLG-2 $\lambda \in [0,2]$, $\mu \in [0,2]$	1.81	0	75	0.669	0.899	0.835	1.247	1.867	0.0029

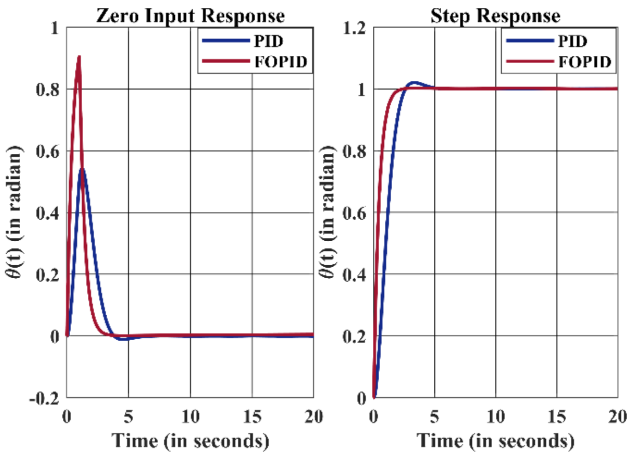

Fig. 129. Comparison of responses of PID and FOPID controller

Although the optimization techniques following some stochastic parameter estimation procedures are easy to implement, they need the initial information regarding the search region. This itself is a problem and is solved by the trial-and-error procedure as the region in which the solution exists is usually unknown. This leads to the need for a deterministic procedure for the evaluation of parameters. This article also examines the loop-shaping method for the tuning of controllers as discussed below.

5.2. Frequency domain loop shaping technique for parameter estimation

The loop transfer function T(s) consisting of the plant G(s), the nonlinear element N(X), and the controller $G_C(s)$ as seen in Figure 9 must satisfy the following frequency-domain design specifications to achieve a better system performance [30].

i. Phase margin specification: The phase margin is associated with the damping and is thereby considered as an index for the system performance. The preceding condition must be satisfied.

$$\begin{aligned} &\mathrm{Arg}[T(j\omega_C)] = -\pi + \phi_m \\ &\text{i.e.}\quad \mathrm{Arg}[G(j\omega_C)G_C(j\omega_C)N(X)] = -\pi + \phi_m \end{aligned} \tag{60}$$

Where, ω_C is the gain cross over frequency, and ϕ_m is the required phase margin.

ii. Gain cross over frequency specifications: It is the means of the stability of the system.

$$\begin{aligned} &|T(j\omega_C)|_{dB} = |G(j\omega_C)G_C(j\omega_C)N(X)|_{dB} = 0\ \ \mathrm{dB} \\ &\text{i.e.}\ |T(j\omega_C)| = |G(j\omega_C)G_C(j\omega_C)N(X)| = 1 \end{aligned} \tag{61}$$

iii. Robustness to gain variations: The robustness of a system towards the gain variation needs the phase angle difference with respect to the frequency to be zero.

$$\begin{aligned} &\frac{d}{d\omega}(\mathrm{Arg}[T(j\omega)])\Big|_{\omega=\omega_C} = 0 \\ &\text{i.e.}\ \frac{d}{d\omega}(\mathrm{Arg}[G(j\omega)G_C(j\omega)N(X)])\Big|_{\omega=\omega_C} = 0 \end{aligned} \tag{62}$$

iv. Rejection of high frequency noise: The robustness of a system to high frequency noise can be attended if the close loop frequency response $P(j\omega)$ satisfies the following low pass filtering requirements.

$$\begin{aligned} &|P(j\omega)|_{dB} \le A_N\ \ \mathrm{dB},\quad \forall\ \ \omega \ge \omega_t \\ &\text{i.e.}\ \left|\left|\frac{G(j\omega)G_C(j\omega)N(X)}{1+G(j\omega)G_C(j\omega)N(X)}\right|_{dB}\right|_{\omega=\omega_t} = A_N\ \ \mathrm{dB} \end{aligned} \tag{63}$$

Where, A_N is the desired noise attenuation value for the cut-off frequency $\omega \ge \omega_t$ rad/s.

v. Rejection of output disturbance: Good disturbance rejection characteristics require fulfillment of the following condition for sensitivity function $S(j\omega)$.

$$\begin{aligned} &|S(j\omega)|_{dB} \le B_D\ \ \mathrm{dB},\quad \forall\ \ \omega \le \omega_s \\ &\text{i.e.}\ \left|\left|\frac{1}{1+G(j\omega)G_C(j\omega)N(X)}\right|_{dB}\right|_{\omega=\omega_s} = B_D\ \ \mathrm{dB} \end{aligned} \tag{64}$$

Where, B_D is the desired sensitivity function value for the cut-off frequency $\omega \le \omega_S$ rad/s.

The above-formulated optimization problem (60-64) is nonconvex and therefore its analytical solution is difficult. Due to the presence of local minima, it is necessary to carry out this problem with several initial guesses. MATLAB optimization toolbox fmincon() with the interior-point algorithm can be utilized to solve this constraint nonlinear optimization problem and gather the optimal. Therefore, with the above constraints considering the robustness to gain variation (62) as the objective function, the modelling of integer and fractional order PID is explained below.

5.2.1. Design of integer-order PID controllers

The phase margin specification (60) reveals the following:

$$\begin{aligned} &-\tan^{-1}\left(\frac{0.2025\omega_C{}^3-1.025\omega_C}{20.2522\omega_C{}^2}\right) + \tan^{-1}\left(\frac{K_D\omega_C{}^2-K_I}{\omega_C K_P}\right) - \\ &\tan^{-1}\left(\frac{\cos^2\beta}{\frac{\pi}{2}+\beta+0.5\sin(2\beta)}\right) - 0.01\omega_C = -\pi+\phi_m \end{aligned} \tag{65}$$

The above equation can be expressed as:

$$\begin{aligned} &\left(\frac{\left\{\frac{\pi}{2}+\beta+0.5\sin(2\beta)\right\}\{(\omega_C K_P)P-(K_D\omega_C{}^2-K_I)Q\} + (\cos^2\beta)[(\omega_C K_P)Q+(K_D\omega_C{}^2-K_I)P]}{\left\{\frac{\pi}{2}+\beta+0.5\sin(2\beta)\right\}\{(\omega_C K_P)Q+(K_D\omega_C{}^2-K_I)P\} - (\cos^2\beta)\{(\omega_C K_P)P-(K_D\omega_C{}^2-K_I)Q\}}\right) + \\ &\{\tan(\phi_m+0.01\omega_C)\} = 0 \end{aligned} \tag{66}$$

Where, $P = 0.2025\omega_C^3 - 1.025\omega_C$, and $Q = 20.2522\omega_C^2$ respectively. Again, the gain crossover frequency constraint (61) can be derived as:

$$\frac{\frac{0.6}{\pi}\left[\sqrt{K_P^2+\left(K_D\omega_C-\frac{K_I}{\omega_C}\right)^2}\right]\left[\sqrt{\left(\frac{\pi}{2}+\beta+0.5\sin(2\beta)\right)^2+\cos^4\beta}\right]}{\sqrt{(20.2522\omega_C^2)^2+(0.2025\omega_C^3-1.025\omega_C)^2}} = 1 \qquad (67)$$

It could further be expressed as:

$$\frac{0.36\left[K_P^2+\left(K_D\omega_C-\frac{K_I}{\omega_C}\right)^2\right]\left[\left(\frac{\pi}{2}+\beta+0.5\sin(2\beta)\right)^2+\cos^4\beta\right]}{\pi^2\sqrt{(20.2522\omega_C^2)^2+(0.2025\omega_C^3-1.025\omega_C)^2}} = 1 \qquad (68)$$

Similarly, the constraint (62) for the robustness of the system provides:

$$\begin{aligned}&\frac{d}{d\omega_C}\left[\tan^{-1}\left(\frac{0.2025\omega_C^3-1.025\omega_C}{20.2522\omega_C^2}\right)\right] + \\ &\frac{d}{d\omega_C}\left[\tan^{-1}\left(\frac{K_D\omega_C^2-K_I}{\omega_C K_P}\right)\right] - \\ &\frac{d}{d\omega_C}\left[\tan^{-1}\left(\frac{\cos^2\beta}{\frac{\pi}{2}+\beta+0.5\sin(2\beta)}\right)\right] - \frac{d}{d\omega_C}[0.01\omega_C] = 0\end{aligned} \qquad (69)$$

As the factor $\frac{d}{d\omega_C}\left[\tan^{-1}\left(\frac{\cos^2\beta}{\frac{\pi}{2}+\beta+0.5\sin(2\beta)}\right)\right] = 0$, the above equation could be further simplified as follows.

$$\begin{aligned}&\left\{\frac{4.1011\omega_C^4 + 20.7585\omega_C^2}{(20.2522\omega_C^2)^2 + (0.2025\omega_C^3 - 1.025\omega_C)^2}\right\} \\ &- \left\{\frac{\omega_C^2 K_P K_D + K_P K_I}{(\omega_C K_P)^2 + (K_D\omega_C^2 - K_I)^2}\right\} + 0.01 = 0\end{aligned} \qquad (70)$$

In this paper instead of random initial guesses, the results obtained from optimization techniques are used as initial guess values assuming (70) as the objective function and (66,68) as the nonlinear equality constraints.

Assuming gain cross-over frequency $\omega_C = 1$ rad/s, phase margins $\phi_m = 60^o, 65^o,$ and 70^o, optimization by the fmincon() solver within the parameter range $K_P \in [0,75]$, $K_I \in [0,75]$, and $K_D \in [0,75]$ provide results as shown in Table 11-13 respectively. It should be noted here that considering (66) or (68) as objective functions did not give optimal results for the controllers toward the quenching of the limit cycle. Hence, that aspect is not included in this article.

Results obtained from the system having a PID controller with different phase margins are compared and shown in Figure 20 and Figure 21. While PID parameters obtained for higher values of ϕ_m quenches the limit cycle but shows marginal sluggish behavior. Thus, the desired limit cycle minimizing controller was obtained for $\phi_m = 60^o$ is:

$$G_C(s) = 56.3399 + \frac{0.0050}{s} + 74.9992\ s \qquad (71)$$

Table 11. PID controller parameters obtained for fmincon optimization technique

Initial Guess Value (From Optimization Techniques)			**Converged Value (From FMINCON) $\phi_m = 60^o$**			**Performance Index**
K_P	K_I	K_D	K_P	K_I	K_D	Obj. Function
75	0	56.22	9.5059	34.4001	75	-0.5276
74.91	0.019	69.09	56.3834	0	75	-0.40981
75	0	60.40	9.5059	34.4001	75	-0.5276
72.69	0	74.99	9.5059	34.4001	75	-0.5276
72.56	0	75	**56.3399**	**0.0050**	**74.9992**	**-0.40978**

Table 12. PID controller parameters obtained for fmincon optimization technique

Initial Guess Value (From Optimization Techniques)			**Converged Value (From FMINCON) $\phi_m = 65^o$**			**Performance Index**
K_P	K_I	K_D	K_P	K_I	K_D	Obj. Function
75	0	56.228	**46.6342**	**0**	**75**	**-0.3779**
74.916	0.019	69.097	49.9080	0	75	-0.3907
75	0	60.409	47.9776	0	75	-0.3834
72.69	0	74.997	51.9944	0	75	-0.3977
72.56	0	75	50.0958	0.0055	74.9998	-0.3914

Table 13. PID controller parameters obtained for fmincon optimization technique

Initial Guess Value (From Optimization Techniques)			**Converged Value (From FMINCON) $\phi_m = 70^o$**			**Performance Index**
K_P	K_I	K_D	K_P	K_I	K_D	Obj. Function
75	0	56.228	**40.2287**	**0**	**75**	**-0.34603**
74.916	0.019	69.097	47.1076	0	75	-0.3799
75	0	60.409	40.2291	0	75	-0.34603
72.69	0	74.997	47.8682	0	75	-0.3830
72.56	0	75	46.1474	0	75	-0.37581

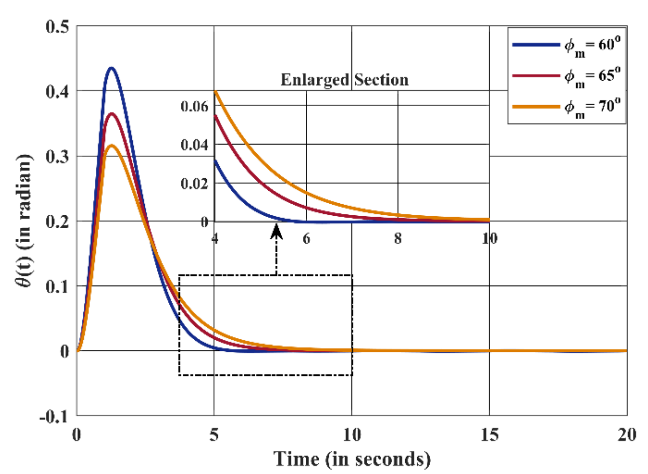

Fig. 20. Comparison of zero input response with backlash nonlinearity and PID controllers

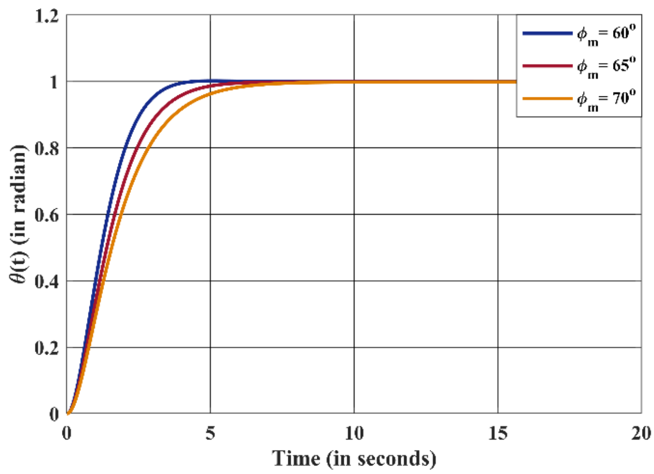

Fig. 21. Comparison of step input response with backlash nonlinearity and PID controllers

5.2.2. Design of $PI^{\lambda}D^{\mu}$ controllers

Similarly, the phase margin specification (60) provides the following relationship:

$$-\tan^{-1}\left(\frac{0.2025\omega_C{}^3-1.025\omega_C}{20.2522\omega_C{}^2}\right)+\tan^{-1}\left(\frac{K_D\omega^{\mu}\sin\frac{\mu\pi}{2}-\frac{K_I}{\omega^{\lambda}}\sin\frac{\lambda\pi}{2}}{K_P+\frac{K_I}{\omega^{\lambda}}\cos\frac{\lambda\pi}{2}+K_D\omega^{\mu}\cos\frac{\mu\pi}{2}}\right)-\tan^{-1}\left(\frac{\cos^2\beta}{\frac{\pi}{2}+\beta+0.5\sin(2\beta)}\right)-0.01\omega_C=-\pi+\phi_m \quad (72)$$

The above equation can be simplified as:

$$\left(\frac{\left\{\frac{\pi}{2}+\beta+0.5\sin(2\beta)\right\}\{AP-BQ\}+(\cos^2\beta)\{AQ+BP\}}{\left\{\frac{\pi}{2}+\beta+0.5\sin(2\beta)\right\}\{AQ+BP\}-(\cos^2\beta)\{AP-BQ\}}\right)+[\tan(\phi_m+0.01\omega_C)]=0 \quad (73)$$

Where, $P = 0.2025\omega_C{}^3-1.025\omega_C$, $Q = 20.2522\omega_C{}^2$, $A = K_P+\frac{K_I}{\omega^{\lambda}}\cos\frac{\lambda\pi}{2}+K_D\omega^{\mu}\cos\frac{\mu\pi}{2}$, and $B = K_D\omega^{\mu}\sin\frac{\mu\pi}{2}-\frac{K_I}{\omega^{\lambda}}\sin\frac{\lambda\pi}{2}$ respectively.

Again, the constraint (61) for gain crossover frequency can be expressed as follows:

$$\frac{\frac{0.6}{\pi}\left\{\sqrt{A^2+B^2}\right\}\left\{\sqrt{\left(\frac{\pi}{2}+\beta+0.5\sin(2\beta)\right)^2+\cos^4\beta}\right\}}{\sqrt{(20.2522\omega_C{}^2)^2+(0.2025\omega_C{}^3-1.025\omega_C)^2}}=1 \quad (74)$$

It can further be simplified as:

$$\frac{0.36\ \{A^2+B^2\}\left\{\left(\frac{\pi}{2}+\beta+0.5\sin(2\beta)\right)^2+\cos^4\beta\right\}}{\pi^2\{(20.2522\omega_C{}^2)^2+(0.2025\omega_C{}^3-1.025\omega_C)^2\}}=1 \quad (75)$$

Likewise, the robustness constraint (62) of the system gives the following equation.

$$\frac{d}{d\omega_C}\left[\tan^{-1}\left(\frac{0.2025\omega_C{}^3-1.025\omega_C}{20.2522\omega_C{}^2}\right)\right]+\frac{d}{d\omega_C}\left[\tan^{-1}\left(\frac{K_D\omega^{\mu}\sin\frac{\mu\pi}{2}-\frac{K_I}{\omega^{\lambda}}\sin\frac{\lambda\pi}{2}}{K_P+\frac{K_I}{\omega^{\lambda}}\cos\frac{\lambda\pi}{2}+K_D\omega^{\mu}\cos\frac{\mu\pi}{2}}\right)\right]-\frac{d}{d\omega_C}\left[\tan^{-1}\left(\frac{\cos^2\beta}{\frac{\pi}{2}+\beta+0.5\sin(2\beta)}\right)\right]-\frac{d}{d\omega_C}[0.01\omega_C]=0 \quad (76)$$

Being independent of ω_C,

$$\frac{d}{d\omega_C}\left[\tan^{-1}\left(\frac{\cos^2\beta}{\frac{\pi}{2}+\beta+0.5\sin(2\beta)}\right)\right]=0 \quad (77)$$

Hence, the above equation is simplified as:

$$\left\{\frac{4.1011\omega_C{}^4+20.7585\omega_C{}^2}{(20.2522\omega_C{}^2)^2+(0.2025\omega_C{}^3-1.025\omega_C)^2}\right\}-\left(\frac{AE-BF}{A^2+B^2}\right)+0.01=0 \quad (78)$$

Where $E = K_D\mu\omega^{\mu-1}\sin\frac{\mu\pi}{2}+\frac{K_I\lambda}{\omega^{\lambda+1}}\sin\frac{\lambda\pi}{2}$ and $F = K_D\mu\omega^{\mu-1}\cos\frac{\mu\pi}{2}-\frac{K_I\lambda}{\omega^{\lambda+1}}\cos\frac{\lambda\pi}{2}$ respectively.

The high-frequency noise reduction constraint (63) makes the following equation:

$$\left.\frac{0.6\sqrt{A^2+B^2}\sqrt{\left(\frac{\pi}{2}+\beta+0.5\sin(2\beta)\right)^2+\cos^4\beta}}{\pi\sqrt{P^2+Q^2}+0.6\sqrt{A^2+B^2}\sqrt{\left(\frac{\pi}{2}+\beta+0.5\sin(2\beta)\right)^2+\cos^4\beta}}\right|_{\omega=\omega_t}-10^{\frac{A_N}{20}}=0 \quad (79)$$

The criterion (64) for disturbance rejection reveals:

$$\left.\frac{\pi\sqrt{P^2+Q^2}}{\pi\sqrt{P^2+Q^2}+0.6\sqrt{A^2+B^2}\sqrt{\left(\frac{\pi}{2}+\beta+0.5\sin(2\beta)\right)^2+\cos^4\beta}}\right|_{\omega=\omega_s}-10^{\frac{B_D}{20}}=0 \quad (80)$$

Likewise, the above-formulated optimization problem is nonconvex, and therefore its analytical solution is difficult. The results obtained from optimizations are used as initial guess values assuming (78) as the objective function and (73, 75, 79, and 80) as the nonlinear equality constraints. Now, by assuming the gain cross-over frequency $\omega_C = 1$ rad/s, the phase margins $\phi_m = 60^o, 65^o$, and 70^o, the required noise attenuation $A_N = -10$ dB for $\omega \geq \omega_t = 10$ rad/s, the value of the sensitivity function $B_D = -20$ dB for $\omega \leq \omega_s = 0.001$ rad/s; the cost minimization by the function fmincon() within the parameter range $K_P \in [0,75]$, $K_I \in [0,75]$, $K_D \in [0,75]$, $\lambda \in [0,1]$, and $\mu \in [0,1]$ provide the following results as shown in Table 14-16 respectively. Again, the results obtained from the system having an FOPID controller with different phase margins are compared and presented in Figure 22 and Figure 23 respectively.

It must be noted here that considering (73) or (75) as the main cost function and the remaining two as nonlinear constraints, did not provide optimal performance of the fractional controllers towards the suppression of the limit cycle. Hence, that aspect of controller design is not included in this paper. While the FOPID parameters obtained for $\phi_m = 60^o, 65^o, 70^o$ are almost similar. The desired limit cycle minimizing FOPID controller thus evaluated for $\phi_m = 70^o$ and is expressed as follows:

$$G_C(s) = 3.8273 + \frac{0.7578}{s^{0.0001}} + 73.9489\ s^{0.9998} \tag{81}$$

Table 14. FOPID controller parameters obtained for fmincon optimization technique

		Constrained Nonlinear Minimization-FMINCON (Phase Margin $\phi_m = 60^o$)			
Initial Guess Values (From Optimization Techniques)	K_P	13.32	73.681	3.8581	73.095
	K_I	0	75	0.6937	74.5
	K_D	75	74.951	75	74.97
	λ	0.6048	0	0.0058	0
	μ	0.9999	1	0.9999	1
Converged Values (From fmincon)	K_P	9.2418	73.7956	**5.9258**	73.118
	K_I	3.0640	74.0868	**4.0862**	74.541
	K_D	58.5145	75	**68.521**	75
	λ	0.6153	0.8710	**0.0011**	0.8724
	μ	1	1	**0.9840**	1
Objective Function		-0.1505	-1.4905	**-0.0693**	-1.5092

Table 15. FOPID controller parameters obtained for fmincon optimization technique

		Constrained Nonlinear Minimization-FMINCON (Phase Margin $\phi_m = 65^o$)			
Initial Guess Values (From Optimization Techniques)	K_P	13.32	73.681	3.8581	73.095
	K_I	0	75	0.6937	74.5
	K_D	75	74.951	75	74.97
	λ	0.6048	0	0.0058	0
	μ	0.9999	1	0.9999	1
Converged Values (From fmincon)	K_P	16.0553	73.7950	**0.0001**	73.1178
	K_I	0.0949	74.0870	**7.9692**	74.5411
	K_D	72.0922	75	**70.1317**	75
	λ	0.0011	0.8702	**0.0011**	0.8716
	μ	1	1	**1**	1
Objective Function		-0.1428	-1.488	**-0.0418**	-1.5066

Table 16. FOPID controller parameters obtained for fmincon optimization technique

		Constrained Nonlinear Minimization-FMINCON (Phase Margin $\phi_m = 70^o$)			
Initial Guess Values (From Optimization Techniques)	K_P	13.32	73.681	3.8581	73.095
	K_I	0	75	0.69372	74.5
	K_D	75	74.951	75	74.97
	λ	0.6048	0	0.0058	0
	μ	0.9999	1	0.9999	1
Converged Values (From fmincon)	K_P	15.7794	73.7941	**3.8273**	73.1174
	K_I	0.1052	74.0872	**0.7578**	74.5411
	K_D	72.2834	75	**73.9489**	75
	λ	0.0009	0.8689	**0.0001**	0.8703
	μ	0.9999	1	**0.9998**	1
Objective Function		-0.13912	-1.4842	**0.0087**	-1.5027

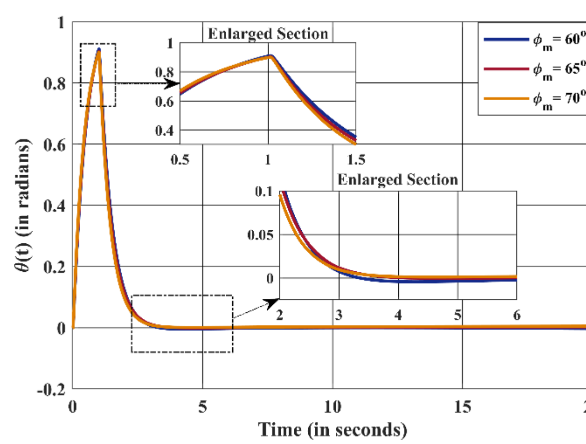

Fig. 22. Comparison of zero input response with backlash nonlinearity and FOPID controllers

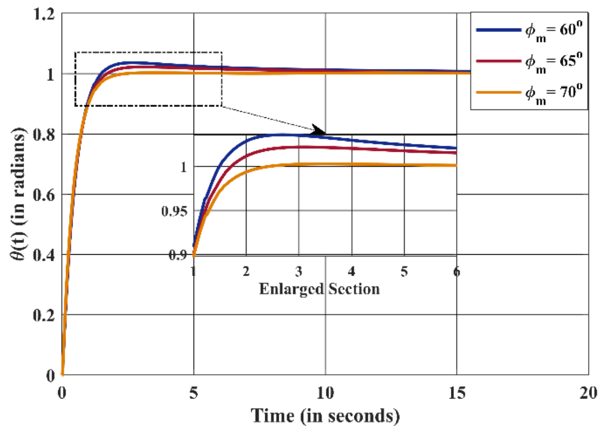

Fig. 23. Comparison of step input response with backlash nonlinearity and FOPID controllers

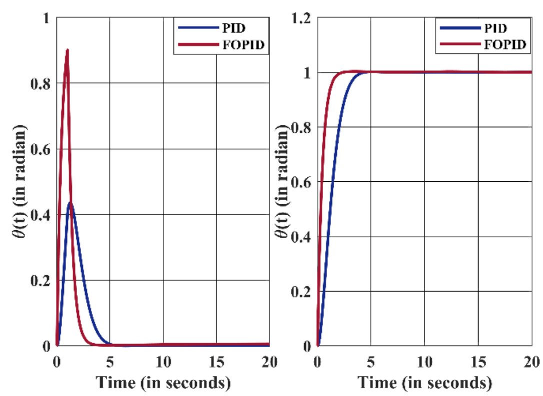

Fig. 24. Comparison of responses of PID and FOPID controllers

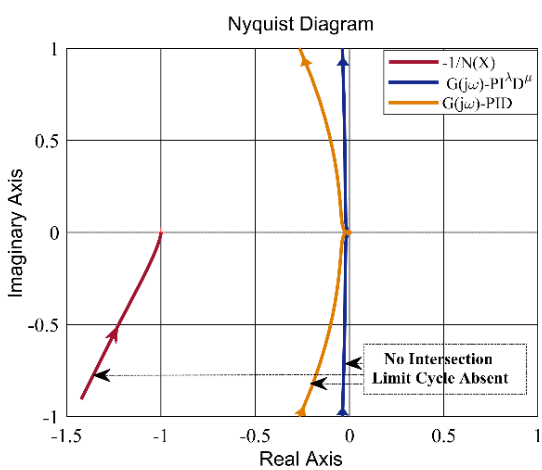

Fig. 25. Superimposed Nyquist plot of G(jω) and Negative inverse plot of N(X) for Backlash with PID and FOPID controllers

Comparison between zero input and step responses of the system with PID and FOPID are shown in Figure 24. Although $PI^{\lambda}D^{\mu}$ the controller shows a significant peek as compared to PID controllers but the settling time is marginally small; thereby proving the superiority of $PI^{\lambda}D^{\mu}$ controllers over the integer-order PID controllers. The overlapped Nyquist and negative inverse figure also confirm no intersection and thereby predict the complete elimination of limit cycle oscillations as seen in Figure 25.

Table 17. Time domain specifications with and without controllers

Time Domain Specifications	Original System	Optimization Method		Loop Shaping Method	
		PID	FOPID	PID	FOPID
Rise Time (T_R) (in seconds)	6.8734	1.5855	**0.9277**	2.1361	0.9415
Settling Time (T_S) (in seconds)	499.14	3.4088	**1.6244**	3.4819	1.6338
Percentage Overshoot M_p(%)	58.03	2.0127	0.1912	0.1252	0.2388
Peak Time (T_P) (in seconds)	18.60	3.3215	3.4572	5.1100	3.4806
Steady State Error (E_{SS})	0.1747	0.0001	0.0006	0.0006	0.0006

The comparison of the time specifications between the PID and FOPID obtained from both the discussed procedures is provided in Table 17. As per expectation, the superiority of fractional controllers can be noticed in terms of rise time and settling time. The major issue with this procedure is the need for an initial guess of solutions. This creates a problem as any random guess might not converge. If the initial guess of the solution is proper, results will be appropriate, else not. Further, the solution also depends upon the GM, PM, and gain cross-over frequency details; which must be obtained by a trial-and-error procedure. Further, it requires five constraints to simplify and solve those nonlinear equations usually the nonlinear optimization toolbox fmincon() is used.

6. Robustness Analysis of the System

The robustness of a control system is usually evaluated against parameter variation and disturbance rejection. In this paper, the usefulness of the proposed controllers is examined based on variations in time delays as well as variations in backlash amplitude. As the prime aim of this article is to minimize the effect on the limit cycle, the zero-input plant response is considered instead of the step output response of the plant.

6.1. Effect of controllers on variation in delay times

The system of Figure 13 is tested against variations in delay times which could inherently be present in the system. The effectiveness of the controller in suppressing the effect of this parameter variation is shown below. It is noticed in Figure 26 that for a time delay of 0.1 s, both controllers work effectively. But for a delay time of 0.5 s, the PID is unable to quench the limit cycle while the FOPID is suppressing the limit cycle efficiently as seen in Figure 27.

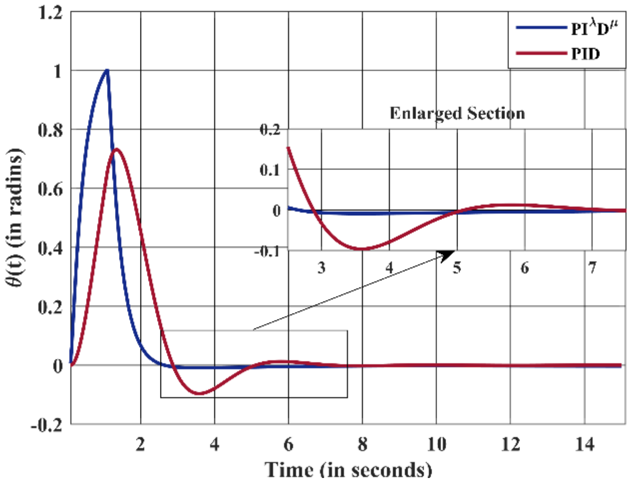

Fig. 26. Zero input response with different controllers considering a delay time of 0.1s

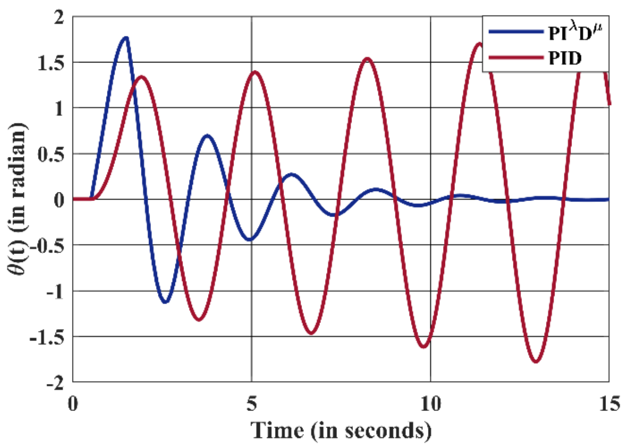

Fig. 27. Zero input response with different controllers considering a delay time of 0.5 s

6.2. Effect of controllers on variable backlash magnitudes

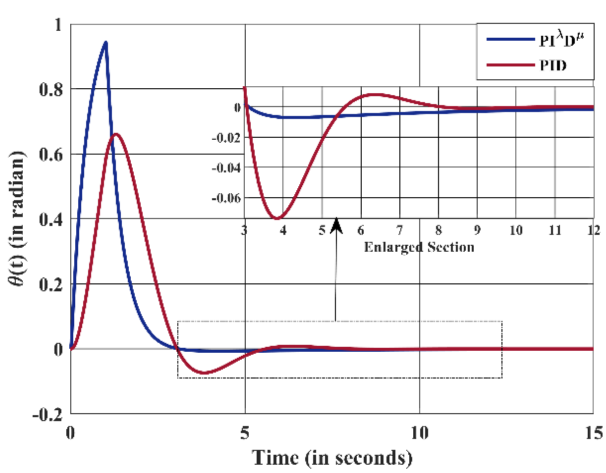

Fig. 28. Zero input response with different controllers considering a backlash amplitude H = 0.005

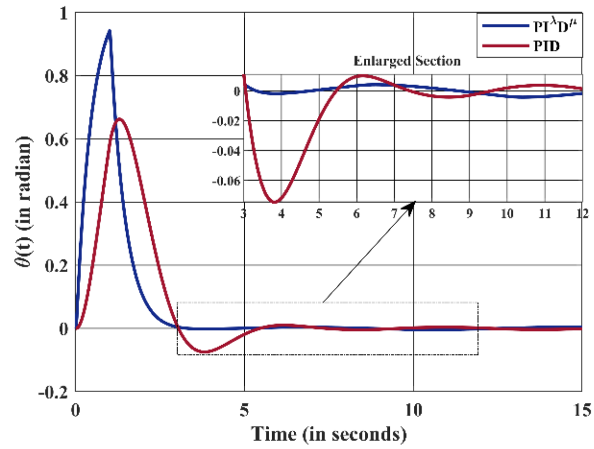

Fig. 29. Zero input response with different controllers considering a backlash amplitude H = 0.25

Likewise, the system of Figure 13 is tested against variations in the backlash magnitude that may arise in the system due to the ageing effect.

The effectiveness of the proposed controllers in eliminating the effect of such variations is demonstrated in Figure 28 and Figure 29 respectively. For every variation in backlash amplitude, the PID and FOPID are seen to eliminate the limit cycle oscillations efficiently. The zero-input response of the plant signifies the dominance of $PI^{\lambda}D^{\mu}$ controllers in terms of robustness to parameter variations against their integer-order counterparts.

7. Realization of the Controllers

The results of integer and non-integer order controllers obtained in the previous sections need to be implementable in real practice. Further, to carry out simulations in MATLAB, the controllers need to be practically realized as mentioned below.

i. The PID controller calculated during the optimization process is found to be a PD controller and can be implemented as follows.

$$G_C(s) = K_P + K_D s = 72.69 + 74.997s \qquad (82)$$

The above improper transfer function can be converted into a proper transfer function by considering the filter coefficient N_F [17]. Let $N_F = 1000$, and therefore the above PD controller can be expressed as:

$$G_C(s) = K_P + K_D s\left(\frac{N_F}{s + N_F}\right) \qquad (83)$$

$$\Rightarrow G_C(s) = 72.69 + 74.997s\left(\frac{1000}{s + 1000}\right) \qquad (84)$$

ii. Likewise, the $PI^{\lambda}D^{\mu}$ controller evaluated during the optimization process can be implementable as mentioned below. The improper fractional differentiator $\mathrm{K_D s^{\mu}}$ can be made a proper function with a fractional filter $N_F = 1000$ as follows:

$$\mathrm{G_C(s)} = \mathrm{K_P} + \frac{\mathrm{K_I}}{\mathrm{s^{\lambda}}} + \mathrm{K_D s^{\mu}} \left(\frac{N_F}{\mathrm{s^{\mu}} + N_F}\right) \tag{85}$$

$$\Rightarrow \mathrm{G_C(s)} = 3.8581 + \frac{0.6937}{\mathrm{s^{0.0058}}} + 75\ \mathrm{s^{0.9998}} \left(\frac{1000}{\mathrm{s^{0.9998}} + 1000}\right) \tag{86}$$

Further, using the Oustaloup filter of order $N = 5$ within the frequency range $[10^{-3}, 10^{-3}]$ rad/s, the fractional elements can be realized. The MATLAB function oustafod$(\beta, N, \omega_b, \omega_h)$ is used for this purpose.

Therefore, for $\mathrm{s^{0.0058}}$ the relevant integer order model is:

$$\mathrm{s^{0.0058}} = \frac{\begin{gathered}1.041s^{11}+773.9s^{10}+1.275e05s^{9}+5.631e06s^{8}+6.962e07s^{7}+\\ 2.44e08s^{6}+2.431e08s^{5}+6.886e07s^{4}+5.529e06s^{3}+\\ 1.243e05s^{2}+748.9s+1\end{gathered}}{\begin{gathered}s^{11}+748.9s^{10}+1.243e05s^{9}+5.529e06s^{8}+6.962e07s^{7}+\\ 2.431e08s^{6}+2.44e08s^{5}+6.962e07s^{4}+5.631e06s^{3}+\\ 1.275e05s^{2}+773.9s+1.041\end{gathered}} \tag{87}$$

Likewise, for $\mathrm{s^{0.9998}}$ the integer order model is:

$$\mathrm{s^{0.9998}} = \frac{\begin{gathered}998.6s^{11}+3.977e05s^{10}+3.511e07s^{9}+\ 8.304e08s^{8}+5.5e09s^{7}+\\ 1.033e10s^{6}+5.511e09s^{5}+8.363e08s^{4}+3.597e07s^{3}+\\ 4.333e05s^{2}+1398s+1\end{gathered}}{\begin{gathered}s^{11}+1398s^{10}+4.333e05s^{9}+3.597e07s^{8}+8.363e08s^{7}+\\ 5.511e09s^{6}+1.033e10s^{5}+5.5e09s^{4}+8.304e08s^{3}+\\ 3.511e07s^{2}+3.977e05s+998.6\end{gathered}} \tag{88}$$

Further, the fractional element $\mathrm{s^{0.0001}}$ can be realized as:

$$\mathrm{s^{0.0001}} = \frac{\begin{gathered}1.001s^{11}+746.7\ \ e05s^{10}+1.235e05s^{9}+\ 5.472e06s^{8}+\\ 6.79e07s^{7}+2.388e08s^{6}+2.388e08s^{5}+6.789e07s^{4}+5.47e06s^{3}+\\ 1.234e05s^{2}+746.2s+1\end{gathered}}{\begin{gathered}s^{11}+746.2s^{10}+1.234e05s^{9}+5.47e06s^{8}+6.789e07s^{7}+\\ 2.388e08s^{6}+2.388e08s^{5}+6.79e07s^{4}+5.472e06s^{3}+\\ 1.235e05s^{2}+746.7s+1.001\end{gathered}} \tag{89}$$

After realization, further analysis or simulation of the fractional elements can be carried out by considering the above model.

8. Conclusion

In this paper, the limit cycle prediction is carried out for a DC servo plant with time delay and backlash nonlinearity. An analytical method based on the DF analysis followed by a Nyquist contour-based graphical procedure and further digital simulations is carried out for the investigation of the possible limit cycle oscillations. The effect of parameter variation on the limit cycle is examined by applying multiple time delays and various backlash magnitudes. Results reveal an increment of oscillation amplitude with a corresponding enhancement in system parameters whereas the frequency of oscillation almost remains the same. PID and FOPID controllers with optimal parametric values are considered for the suppression of these limit cycle oscillations. Parameter estimation of the controller is carried out using optimization methods by minimizing performance indices as well as by adopting a frequency domain-based loop shaping approach.

In the optimization-based procedure, statistical studies reveal the superiority of MFO over other applied algorithms towards the minimization of the cost functions and providing desired system performance in terms of suppression of limit cycle oscillations. While the superiority of MFO-tuned ITAE is noticed for PID controllers, the MFO-tuned ITSE provides superior performance for FOPID controllers. In the analytical procedure, out of the five applied loop shaping constraints, the robustness to gain variations condition provided better results being an objective function and the other four as nonlinear constraints for different values of phase margins.

Further, the simulation results reveal the authenticity of the PID and FOPID controllers in suppressing the oscillation magnitude and capturing the desired closed-loop system performance. Robustness studies clearly show the effectiveness of the controllers towards system parameter variations. It further indicates the superiority of FOPID controllers in terms of achieving desired system performance as well as insensitivity towards the system parameter variations.

Conflict of Interest

The corresponding author assures no conflict of interest on behalf of all the authors.

Data Availability

On behalf of all authors, the corresponding author agrees to make the research data available upon reasonable request.

CRediT Author Statement

Biresh Kumar Dakua: Conceptualization, Writing-original draft, Validation, Data curation
Bibhuti Bhusan Pati: Supervision, Formal analysis

References

[1] Atherton DP. Nonlinear control engineering. Van Nostrand Rheinhold. 1975. ISBN:9780442300173.

[2] Gopal M. Control systems: principles and design. McGraw-Hill Science, Engineering & Mathematics; 2008. ISBN: 9780073529516.

[3] Dakua BK, Pati BB. Prediction and suppression of limit cycle oscillation for a plant with time delay and backlash nonlinearity. In2020 IEEE International Symposium on Sustainable Energy, Signal Processing and Cyber Security (iSSSC) 2020 Dec 16 (pp. 1-5). IEEE. https://doi.org/10.1109/iSSSC50941.2020.9358900.

[4] Kesarkar AA, Selvaganesan N, Priyadarshan H. A novel framework to design and compare limit cycle minimizing controllers: demonstration with integer and fractional-order controllers. Nonlinear Dynamics. 2014; 78: 2871-82. https://doi.org/10.1007/s11071-014-1632-6.

[5] Kesarkar AA, Selvaganesan N, Priyadarshan H. Novel controller design for plants with relay nonlinearity to reduce amplitude of sustained oscillations: Illustration with a fractional controller. ISA transactions. 2015;57:295-300. https://doi.org/10.1016/j.isatra.2015.01.005.

[6] Perumal S, Selvaganesan N. Input dependent Nyquist plot for limit cycle prediction and its suppression using fractional order controllers. Transactions of the Institute of Measurement and Control. 2019;41(13) 3847-60. https://doi.org/10.1177/0142331219841113.

[7] Mbitu ET, Chen SC. Designing limit-cycle suppressor using dithering and dual-input describing function methods. mathematics. 2020;8(11):1978. https://doi.org/10.3390/math8111978.

[8] Yeroglu C, Tan N. Limit cycle prediction for fractional order systems with static nonlinearities. IFAC Proceedings Volumes. 2010;43(11):144-9. https://doi.org/10.3182/20100826-3-TR-4016.00029.

[9] Atherton DP, Tan N, Yeroglu C, Kavuran G, Yüce A. Limit cycles in nonlinear systems with fractional order plants. Machines. 2014;2(3):176-201. https://doi.org/10.3390/machines2030176.

[10] Atherton DP, Tan N, Yeroglu C, Kavuran G, Yüce A. Computation of limit cycles in nonlinear feedback loops with fractional order plants. InICFDA'14 International Conference on Fractional Differentiation and Its Applications 2014. Jun 23 (pp. 1-6). IEEE. https://doi.org/10.1109/ICFDA.2014.6967404.

[11] Yüce A, Tan N, Atherton DP. Limit cycles in relay systems with fractional order plants. Transactions of the Institute of Measurement and Control. 2019;41(15):4424-35. https://doi.org/10.1177/0142331219860302.

[12] Dakua BK, Pati BB. Computation of Limit Cycle in a Nonlinear Fractional-Order Feedback Control Plant with Time Delay. In2021 1st Odisha International Conference on Electrical Power Engineering, Communication and Computing Technology (ODICON) 2021 Jan 8 (pp. 1-6). IEEE. https://doi.org/10.1109/ODICON50556.2021.9428950.

[13] Patra KC, Dakua BK. Investigation of limit cycles and signal stabilization of two dimensional systems with memory type nonlinear elements. Archives of Control Sciences. 2018;2:285-330. https://doi.org/10.24425/123461.

[14] Patra KC, Kar N. Suppression limit cycles in 2× 2 nonlinear systems with memory type nonlinearities. International Journal of Dynamics and Control. 2022;10(3):721-33. https://doi.org/10.1007/s40435-021-00860-x.

[15] Patra KC, Patnaik A. Investigation of the Existence of Limit Cycles in Multi Variable Nonlinear Systems with Special Attention to 3X3 Systems. Int. Journal of Applied Mathematics, Computational Science and System Engineering. 2023;5:93-114. https://doi.org/10.37394/232026.2023.5.9.

[16] Patra KC, Patnaik A. Possibility of Quenching of Limit Cycles in Multi Variable Nonlinear Systems with Special Attention to 3X3 Systems. WSEAS Transactions on Systems and Control. 2023;18:677-95. https://doi.org/10.37394/23203.2023.18.69.

[17] Cominos P, Munro N. PID controllers: recent tuning methods and design to specification. IEE Proceedings-Control Theory and Applications. 2002;149(1):46-53. https://doi.org/10.1049/ip-cta:20020103.

[18] Petráš I. Fractional-order nonlinear systems: modeling, analysis and simulation. Springer Science & Business Media; 2011 May 30. ISSN 1867-8440.

[19] Boudjelıda L, Hisar Ç, Sefa I. Design and Control of a Permanent Magnet Assisted Synchronous Reluctance Motor. International Journal of Automotive Science and Technology. 2023;7(4):332-9. https://doi.org/10.30939/ijastech..1366882.

[20] Kuyu YÇ. Trajectory Tracking Control Using Evolutionary Approaches for Autonomous Driving. International Journal of Automotive Science And Technology. 2024;8(1):110-7. https://doi.org/10.30939/ijastech..1354082.

[21] Karakaş O, Şeker UB, Solmaz H. Modeling of an electric bus Using MATLAB/Simulink and determining cost saving for a realistic city bus line driving cycle. Engineering Perspective. 2021;1(2):52-62. http://dx.doi.org/10.29228/eng.pers.51422.

[22] Arslan TA, Aysal FE, Çelik İ, Bayrakçeken H, Öztürk TN. Quarter Car Active Suspension System Control Using Fuzzy Controller. Engineering Perspective. 2022;2(4):33-9. http://dx.doi.org/10.29228/eng.pers.66798.

[23] Dakua BK, Pati BB. PIλ-PDμController for Suppression of Limit Cycle in Fractional-Order Time Delay System with Nonlinearities. In2021 1st Odisha International Conference on Electrical Power Engineering, Communication and Computing Technology (ODICON) 2021 Jan 8 (pp. 1-6). IEEE. https://doi.org/10.1109/ODICON50556.2021.9428971.

[24] Xue D, Li T, Liu L. A MATLAB toolbox for multivariable linear fractional-order control systems. In2017 29th Chinese Control And Decision Conference (CCDC) 2017 May 28 (pp. 1894-1899). IEEE. https://doi.org/10.1109/CCDC.2017.7978826.

[25] Tepljakov A, Petlenkov E, Belikov J. FOMCON toolbox for modeling, design and implementation of fractional-order control systems. Applications in control. 2019 Feb 19; 6:211-36. https://doi.org/10.1515/9783110571745-010.

[26] Podlubny I. Fractional-order systems and PI/sup/spl lambda//D/sup/spl mu//-controllers. IEEE Transactions on automatic control. 1999;44(1):208-14. https://doi.org/10.1109/9.739144.

[27] Oustaloup A, Levron F, Mathieu B, Nanot FM. Frequency-band complex noninteger differentiator: characterization and synthesis. IEEE Transactions on Circuits and Systems I: Fundamental Theory and Applications. 2000;47(1):25-39. https://doi.org/10.1109/81.817385.

[28] Krishna BT. Studies on fractional order differentiators and integrators: A survey. Signal processing. 2011;91(3):386-426. https://doi.org/10.1016/j.sigpro.2010.06.022.

[29] Krishna BT. Various methods of realization for fractional-order elements. ECTI Transactions on Electrical Engineering,

Electronics, and Communications. 2023;28(1):1-10. https://doi.org/10.37936/ecti-eec.2023211.248544.

[30]Monje CA, Vinagre BM, Feliu V, Chen Y. Tuning and auto-tuning of fractional order controllers for industry applications. Control engineering practice. 2008;16(7):798-812. https://doi.org/10.1016/j.conengprac.2007.08.006.

[31]Yeroglu C, Tan N. Note on fractional-order proportional–integral–differential controller design. IET control theory & applications. 2011 Nov 17;5(17):1978-89. https://doi.org/10.1049/iet-cta.2010.0746.

[32]Deniz FN, Yüce A, Tan N, Atherton DP. Tuning of fractional order PID controllers based on integral performance criteria using Fourier series method. IFAC-PapersOnLine. 2017;50(1):8561-6. https://doi.org/10.1016/j.ifacol.2017.08.1417.

[33]Birs I, Muresan C, Mihai M, Dulf E, De Keyser R. Tuning guidelines and experimental comparisons of sine based auto-tuning methods for fractional order controllers. IEEE Access. 2022;10:86671-83. https://doi.org/10.1109/ACCESS.2022.3198943.

[34]Paducel I, Safirescu CO, Dulf EH. Fractional order controller design for wind turbines. Applied Sciences. 2022;12(17):8400. https://doi.org/10.3390/app12178400.

[35]Ionescu CM, Dulf EH, Ghita M, Muresan CI. Robust controller design: Recent emerging concepts for control of mechatronic systems. Journal of the Franklin Institute. 2020;357(12):7818-44. https://doi.org/10.1016/j.jfranklin.2020.05.046.

[36]Kesarkar AA, Selvaganesan N. Superiority of fractional order controllers in limit cycle suppression. International Journal of Automation and Control. 2013;7(3):166-82. https://doi.org/10.1504/IJAAC.2013.057057.

[37]Dakua BK, Pati BB. A deterministic design approach of tilt integral derivative controller for integer and fractional-order system with time delay. Engineering Research Express. 2024;6(3):035331. https://doi.org/10.1088/2631-8695/ad6ca5.

[38]Kumar P, Chatterjee S, Shah D, Saha UK, Chatterjee S. On comparison of tuning method of FOPID controller for controlling field controlled DC servo motor. Cogent Engineering. 2017;4(1):1357875. https://doi.org/10.1080/23311916.2017.1357875.

[39]Ekinci S, Izci D, Hekimoğlu B. Optimal FOPID speed control of DC motor via opposition-based hybrid manta ray foraging optimization and simulated annealing algorithm. Arabian Journal for Science and Engineering. 2021;46(2):1395-409. https://doi.org/10.1007/s13369-020-05050-z.

[40]Hekimoğlu B. Optimal tuning of fractional order PID controller for DC motor speed control via chaotic atom search optimization algorithm. IEEE access. 2019;7:38100-14. https://doi.org/10.1109/ACCESS.2019.2905961.

[41]Ersali C, Hekimoğlu B. FOPID controller design for a buck converter system using a novel hybrid cooperation search algorithm with pattern search for parameter tuning. Gazi University Journal of Science Part A: Engineering and Innovation. 2023;10(4):417-41. https://doi.org/10.54287/gujsa.1357216.

[42]Mirjalili S, Lewis A. The whale optimization algorithm. Advances in engineering software. 2016;95:51-67. https://doi.org/10.1016/j.advengsoft.2016.01.008.

[43]Kennedy J, Eberhart R. Particle swarm optimization. InProceedings of ICNN'95-international conference on neural networks 1995 Nov 27 (Vol. 4, pp. 1942-1948). ieee. https://doi.org/10.1109/ICNN.1995.488968.

[44]Mirjalili S. The ant lion optimizer. Advances in engineering software. 2015;83:80-98. https://doi.org/10.1016/j.advengsoft.2015.01.010.

[45]Mirjalili S, Mirjalili SM, Lewis A. Grey wolf optimizer. Advances in engineering software. 2014;69:46-61. https://doi.org/10.1016/j.advengsoft.2013.12.007.

[46]Mirjalili S. Moth-flame optimization algorithm: A novel nature-inspired heuristic paradigm. Knowledge-based systems. 2015;89:228-49. https://doi.org/10.1016/j.knosys.2015.07.006.

[47]Gaing ZL. A particle swarm optimization approach for optimum design of PID controller in AVR system. IEEE transactions on energy conversion. 2004;19(2):384-91. https://doi.org/10.1109/TEC.2003.821821.